Lithos 230 (2015) 1–16

Contents lists available at ScienceDirect

Lithos

journal homepage: www.elsevier.com/locate/lithos

The Friningen Garnet Peridotite (central Swedish Caledonides). A good example of the characteristic PTt path of a cold mantle wedge garnet peridotite

Mattia Gilio [a,b,*], Frediano Clos [a,c], Herman L.M. van Roermund [a]

[a] Structural Geology and Tectonics Department of Earth Sciences, Utrecht University, Budapestlaan 4, Utrecht, 3508 TA, The Netherlands
[b] Dipartimento di Scienze della Terra, Ambiente e Vita, University of Genova, Corso Europa 26, 16132 Genova, Italy
[c] School of Geosciences, Monash University, Clayton, VIC 3800, Australia

ARTICLE INFO

Article history:
Received 4 June 2014
Accepted 6 May 2015
Available online 15 May 2015

Keywords:
Mantle wedge garnet peridotite
Characteristic PTt-d path
Archean SCLM
Seve Nappe Complex
Scandinavian Caledonides
Plate interface

ABSTRACT

We present pseudosections of Cr-bearing garnet peridotite that together with new mineral–chemical data allow quantification of the early PT conditions of the original lithospheric mantle assemblage (M1) of the Friningen Garnet Peridotite (FGP) located in the central/middle belt of the Seve Nappe Complex in central Sweden. Results indicate that the early, coarse grained, olivine + orthopyroxene + clinopyroxene + "high Cr" garnet assemblage (M1a) was formed at 1100 ± 100 °C and 5.0 ± 0.5 GPa. These metamorphic conditions were followed by an inferred late Proterozoic exhumation event down to 850–900 °C and 1.5 GPa (M1b). The latter PT estimate is based on the breakdown of high-Cr M1a garnet (Cr# = 0.065) + olivine into an orthopyroxene + clinopyroxene + spinel (Cr# = 0.15–0.25) ± pargasite kelyphite (M1b) and the exsolution of garnet from Al-rich orthopyroxene and clinopyroxene. The M1b kelyphite is overprinted by an early-Caledonian UHPM mineral assemblage (M2; T = 800 °C and P = 3.0 GPa), equivalent to the earlier discovered UHP assemblage within an eclogitic dyke that cross-cuts FGP. In the garnet peridotite M2 is displayed by low-Cr garnet (Cr# = 0.030) growing together with spinel (Cr# = 0.35–0.45), both these minerals form part of the olivine + orthopyroxene + clinopyroxene + garnet + spinel + pargasite M2 assemblage. The formation of plagioclase + diopside symplectites after omphacite and breakdown of kyanite to sapphirine + albite in internal eclogite and the breakdown of M2 olivine + garnet to amphibole + orthopyroxene + spinel assemblages (M3) in garnet peridotite indicate post-UHP isothermal decompression down to 750–800 °C and 0.8–1.0 GPa (=M3). Multiphase solid-and fluid inclusion assemblages composed of Sr-bearing magnesite, dolomite or carbon decorate linear defect structures within M1a–b minerals and/or form subordinate local assemblages together with M2 minerals. The latter are interpreted as evidence for infiltration of early-Caledonian COH-bearing subduction zone fluids. The well-defined PTt-deformation path of the FGP resembles that of a mantle wedge garnet peridotite. The M1 assemblage originates from the base of a cold, old and thick subcontinental lithospheric mantle that is inferred to extend asymmetrically leading to extreme exhumation of FGP down to lithospheric conditions around 1.5 GPa and 850–900 °C. After that the FGP became incorporated into the subducting continental crust of the SNC during "early-Caledonian" subduction (M2) down to UHPM conditions (800 °C/3.0 GPa), subsequently followed by eduction back to sub-crustal levels. As such, FGP is the first locality in the Swedish Caledonides from which two UHP metamorphic events are described, the first event can be related to the formation of an ancient (>1.0 Ga) lithosphere underneath a craton (Rodinia) and the second is of early-Caledonian age.

1. Introduction

Mantle fragments, tectonically introduced into the continental crust during plate collisional processes, are a common feature of major orogenic belts throughout the world (Coleman, 1971; Den Tex, 1969).

In the Scandinavian Caledonides, most orogenic peridotites consist of spinel dunite, harzburgite or serpentinite. However, occurrences exclusively restricted to (U-)HP metamorphic terranes also contain an (ultra-) high pressure garnet–olivine-bearing assemblage (Brueckner, 1977; Brueckner et al., 2010; Carswell et al., 1983; Eskola, 1921; Krogh

Abbreviations: Cr#, (Cr)/(Cr + Al); FGP, Friningen garnet peridotite; KSP, Kittelfjäll spinel peridotite; Mg#, (Mg)/(Mg + Fe); SCLM, sub-continental lithospheric mantle; MW-GP, mantle wedge garnet peridotite; SZ-GP, subduction zone garnet peridotite; WBA, wide beam analyses; SNC, Seve Nappe Complex; UHP, ultra-high pressure; WGC, Western Gneiss Complex.

* Corresponding author at: Dipartimento di Scienze della Terra, Ambiente e Vita, University of Genova, Corso Europa 26, 16132 Genova, Italy.
E-mail addresses: mattia.gilio@edu.unige.it (M. Gilio), frediano.clos@monash.edu (F. Clos), h.l.m.vanroermund@uu.nl (H.L.M. van Roermund).

http://dx.doi.org/10.1016/j.lithos.2015.05.003
0024-4937/

et al., 2006; Medaris, 1984; Spengler, 2006; Spengler et al., 2009; Van Roermund, 1989; Van Roermund and Drury, 1998). An outstanding, though classic, question therefore is: are the garnet–olivine assemblages formed during deep subduction of low pressure peridotites (i.e. chlorite-, plagioclase- or spinel-bearing) and serpentinites, or do these garnet–olivine bearing ultramafic massifs represent fragments of deeper parts of the lithospheric (or asthenospheric) mantle, detached from the mantle-wedge and trapped into the continental crust during deep subduction or eduction processes (Brueckner, 1998)? Thus, garnet peridotites can form by prograde metamorphism after burial and subduction to pressures higher than about 1.6 GPa of Al-bearing ultramafic bodies present in the continental crust prior to subduction or the underlying (low pressure) lithospheric mantle. This type is called subduction zone garnet peridotite (SZgp). Good examples are: 1) prograde serpentinites (Cima di Gagnone, Central Alps; Scambelluri et al., 2014; Trommsdorff and Evans, 1974) and Tromsø Nappe, Scandinavian Caledonides (Krogh et al., 2006), 2) spinel peridotites (Bergen Arcs; Kühn et al., 2000) and Ulten/Nonberg, Italian Alps (Obata and Morten, 1987; Scambelluri et al., 2006), 3) basal sections of layered mafic intrusions i.e. the Fe–Ti subtype of Carswell et al. (1983) with Eiksunddalen in Norway being the prototype (Jamtveit, 1987). Alternatively, during descent as well as re-ascent, in deeper parts of a continental subduction system, the friction between the subducting continental crust and the overlying lithospheric (and asthenospheric) mantle wedge may cause slices of garnet–olivine bearing mantle to get trapped into the descending and ascending plate (Brueckner et al., 2010). These mantle slices would then follow the continental crust during ongoing subduction and eduction. This type of garnet peridotite is called mantle wedge garnet peridotite (MWgp; Van Roermund, 2009). The fundamental importance of MWgp stems from the capabilities of depleted and ultra-depleted peridotite bodies to preserve foliations, textures, mineral compositions and trace element and isotope signatures that precede the (U)HP metamorphic event, while being almost immune to LP metamorphic overprints and deformation phases. Thus, MWgp's form ideal proxies to study medium to large scale lithospheric mantle processes (Zhang et al., 2011) related to structural and chemical geodynamics (Bebout, 2007; Zheng, 2012), i.e. chemical and physical processes that otherwise can only be studied at much smaller scales using mantle xenoliths in basaltic intrusions.

Isolated ultramafic bodies of different dimensions (from km- to cm-scale), composition and metamorphic grade or structure occur in every unit of the Seve Nappe Complex (SNC), central Swedish Caledonides (Bucher-Nurminen, 1991). These orogenic peridotites were traditionally interpreted as fragments of sub-oceanic, Iapetus-related, lithosphere that became incorporated into the Scandian nappe pile during the Caledonian orogeny (Coleman, 1971; Du Rietz, 1935; Qvale and Stigh, 1985; Zwart, 1974). Van Roermund (1989) first challenged this interpretation, describing the occurrence, mineralogy, petrogenesis and tectonic implications of garnet peridotites from a relatively small area in northern Jämtland, central Sweden. The type locality of these garnet peridotites is the Friningen Garnet Peridotite (FGP), exposed in the Central/Middle Belt of the SNC, close to the SE side of Lake Friningen (Fig. 1). Other garnet peridotites also occur in this area.

This study is focused on a detailed description of the fundamental microstructures, mineral compositions, and mutual time relationships among the various mineral assemblages occurring within the FGP body. This is done to define a PTt-d path, which turns out to be characteristic for a MWgp. This study also includes results of the earlier age dating work by Brueckner and Van Roermund (2004, 2007) and the recent discovery of UHPM conditions in a meta-basic dyke cross-cutting the FGP (Janák et al., 2013). However, the latter discovery requires a microstructural and mineralogical correlation between metabasic and ultrabasic rock types present within the FGP. In previous studies, Van Roermund (1989) and Brueckner et al. (2004) did not accurately determine the pre-Caledonian PT conditions of the FGP due to the pervasive resetting of the pre-Caledonian mineral compositions used to calculate their formation conditions. The aim of this work is therefore: 1) to determine the pre-Caledonian mantle conditions of the FGP, 2) to construct a definitive PTt-d path for the FGP and 3) to compare this PTt-d path with that of the associated metabasic rocks (Janák et al., 2013). New results are obtained from thermodynamic modelling. Finally, we present also the fundamental olivine microstructures and fabrics (supplementary material). This is done to calculate flow stress levels operating within the sub-continental lithospheric mantle (SCLM) during Proterozoic, early-Caledonian subduction and subsequent return to sub-crustal levels.

2. Geological background

The overall internal structure of the SNC consists of a number of thrust sheets composed of heterogeneous lithological compositions and variable structural-metamorphic (including UHP) histories (Andréasson, 1994; Gee et al., 2008, 2013; Strömberg et al., 1984; Williams and Zwart, 1977; Zachrisson, 1969; Zachrisson and Stephens, 1984). In northern Jämtland, the SNC directly overlies the low-grade lower Allochthon (not visible in Fig. 1) and it underthrusts the Köli Nappes in the west (Fig. 1). Here, the SNC is divided into three main belts, from top to bottom: the Western, Central and Eastern Belts (Trouw, 1973; Van Roermund and Bakker, 1984; Williams and Zwart, 1977; Zwart, 1974).

The Upper Seve Nappe (Western Belt) consists of garnet bearing quartz–micaschists with local lenses of amphibolite and serpentinite. The Middle Seve Nappe (Central Belt) is formed by several tectonic lenses consisting of migmatitic kyanite–sillimanite gneiss, quartz–feldspar gneiss and (garnet) amphibolite. In one of these lenses, the Ertsekey Lens (also known as Avardo Gneiss; Fig. 1), Van Roermund and Bakker (1984) described eclogites formed at 1.8–2.4 GPa/780 °C and hosted by migmatitic gneisses. Several foliated, lens-shaped, dunite and harzburgite bodies occur, usually close to the contact between the various rock units (Fig. 1). Some of these ultramafic rocks contain the characteristic (U)HP garnet–olivine assemblage. The Lower Seve Nappe (Eastern Belt) consists of garnet-bearing micaschist, kyanite–staurolite schist, quartzo-feldspathic gneiss, amphibolite, quartzite, calc-silicate and garnet–biotite rocks. These rocks do not show any evidence of HP metamorphism or partial melting, except for the Tjeliken Lens (Fig. 1), where eclogites and garnet peridotites occur (Van Roermund, 1985, 1989). According to previous studies by Van Roermund (1985), Tjeliken eclogites were formed around 1.3–1.5 GPa/550–620 °C (Van Roermund, 1985). However, after new methods of calculating PT conditions became available, Majka et al. (2013) determined these conditions to be around 2.7–2.8 GPa/700 °C. Scattered ultramafic bodies are found within all units of the Lower Seve Nappe, two of which, both included in the Tjeliken Lens, contain the HP garnet–olivine assemblage (Van Roermund, 1989).

From top to bottom, the SNC shows first an increase, followed by a decrease in metamorphic grade, with granulite to eclogite facies rocks in the Central/Middle Belt and lower to middle amphibolite facies rocks in the adjacent Eastern/Lower and Western/Upper Belts. The Tjeliken UHP lens forms an exception to this general rule. Another characteristic of metamorphism within the Central/Middle Seve belt is that calculated metamorphic pressure varies along the axis of the Caledonian orogen. Highest pressures occur in the Avardo Gneiss (≥1.8 GPa), intermediate pressures in the Marsfjället gneiss (1.25–1.8 GPa) and lowest pressures in the Lillfjället gneiss (≤1.25 GPa; Fig. 1).

3. Previous investigations of the Friningen Garnet Peridotite

The Friningen Garnet Peridotite (FGP) is a 200 × 30 m sized ultramafic lens occurring within the Central Belt of the SNC, close to the structural top of the eclogite-bearing migmatitic Ky-Sil-Kfs gneiss (Ertsekey lens) near Lake Friningen (Fig. 1). The FGP was first mentioned by Du Rietz (1935) while Van Roermund (1989) made the first detailed field and petrographic description, presented EMP mineral

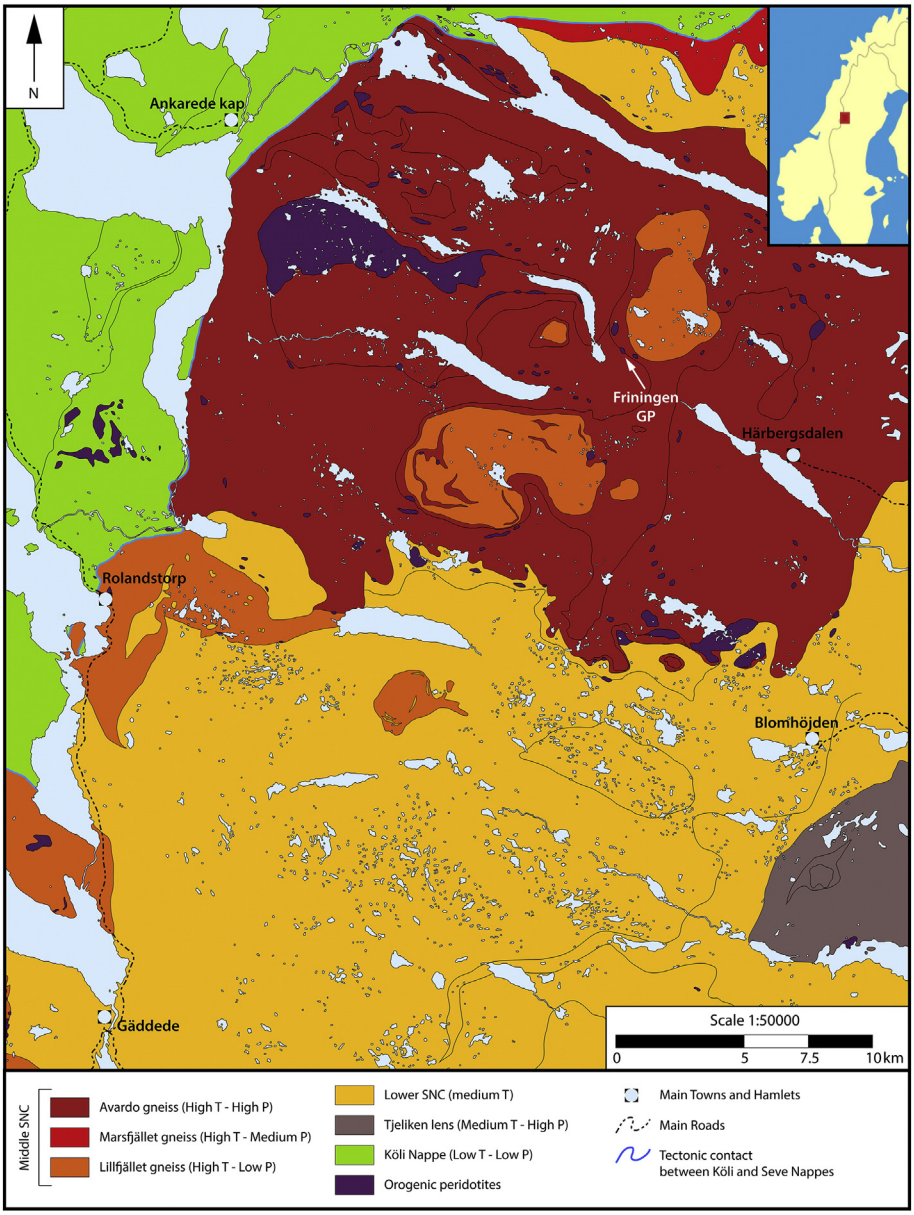

Fig. 1. Metamorphic map of the Seve-Köli Nappe Complex in northern Jämtland, Central Sweden. The black solid lines in the background of the map refer to the main geological units outlined on the geological map presented by Van Roermund (1985). All rock units on the map generally dip (moderately) to the west/north west.

compositions and calculated the PT conditions under which the M2 garnet–olivine assemblage was formed (1.9 ± 0.3 GPa–750 ± 50 °C). For a detailed structural and lithological characterisation of the FGP the reader is referred to Verbaas and Van Roermund (2012).

The body consists of a series of layers with different thicknesses (0.1 to 2–3 m) and bulk rock compositions (ranging from almost pure dunite to garnet lherzolite). A 30 cm thick, boudinaged dyke of garnet pyroxenite, locally containing the eclogitic Ky + Ph + Omp + Grt assemblage (Janák et al., 2013), is concordant with the main foliation of the body. All lithologies are well preserved, without any substantial weathering.

In the FGP, four different foliations can be observed (S_0, S_1, S_2 and S_3). S_0 is a compositional layering defined by the relative modal variation of the major rock-forming minerals (Ol ± Opx ± Cpx ± Grt = M1). In most cases, S_0 is parallel to the S_1 foliation defined by the shape-preferred orientation of the coarse-grained (≤2 cm), highly strained, porphyroclasts of M1a minerals embedded within a fine-grained, dynamically recrystallized matrix defining the M2 (Ol + Opx + Cpx + Grt + Spl + Prg) assemblage. The S_0 and S_1 foliations are locally folded into small and tight to isoclinal folds with the second foliation (S_2) parallel to the axial planes of these folds. In outcrop, the S_2 foliation is generally subparallel to S_0 and S_1 but, locally, it can form angles up to 30°. The S_3 foliation occurs within 10–60 cm thick, non-penetrative, anastomosing, fine grained shear bands cropping out close to the contact with the surrounding migmatitic gneisses.

The three deformation events (D1/S1, D2/S2, and D3/S3) are associated with at least three metamorphic events (M1, M2, and M3). The oldest mineral assemblage (M1a) in the peridotite consists of coarse-grained Ol ± Opx ± Cpx ± Grt (±sulphides of Archean age); their elongate shape is variably aligned according to the S1 foliation. The M1a garnet breaks down into Cpx + Opx + Spl(±Amp) kelyphite (M1b assemblage). A second mineral assemblage (M2) in the peridotite consists of Ol(2) ± Opx(2) ± Cpx/Amp(2) ± Grt(2) ± Spl(2). Recent pressure and temperature (PT) estimates, exclusively based on Fe/Mg partitioning between Grt–Opx and Al-in-Opx, indicated that the M1a assemblage formed at 2.3 GPa/840 °C and the M2 assemblage around 1.8 GPa/800–840 °C (Verbaas and Van Roermund, 2012). Using the same geothermobarometric method, Brueckner et al. (2004), following

Van Roermund (1989), calculated the PT conditions for the M2 assemblage in garnet peridotite and garnet pyroxenite to be 2.0–3.0 GPa/700–800 °C. Recently, Janák et al. (2013) used another technique to calculate PT conditions of 3.0–3.5 GPa/710–810 °C for the kyanite–phengite eclogite assemblage in the metabasic dyke cross-cutting the peridotite body. According to Janák et al. (2013), these PT conditions correspond with the M2 stage of the garnet peridotite. These M2 conditions overlap the M1a conditions of the M1a assemblage reported by Verbaas and Van Roermund (2012). A viable explanation for this is chemical resetting of the pre-Caledonian mineral compositions during the M2 UHP overprint. This topic will be discussed in the present work.

The early Caledonian UHP (M2) metamorphic stage was followed by isothermal decompression (M3) down to 0.8–1.0 GPa/750–850 °C (recorded in eclogite; Janák et al., 2013). Surrounding gneisses (Van Roermund and Bakker, 1984) and external eclogites (Van Roermund, 1985) record similar (M3) PT conditions.

In the FGP, Brueckner et al. (2004) reported three groups of radiometric ages. Re–Os analyses of sulphide (Pentlandite) gave Archean ages which are related to multiple events of partial melting and mantle depletion in Archean time. Sm–Nd clinopyroxene model ages (M1 crystals) from the garnet peridotite and metabasic UHP dyke are Proterozoic (1.1–1.2 Ga). This indicates that at least one refertilization event, coupled to the intrusion of a basic dyke swarm, occurred during the Proterozoic. Finally, Sm–Nd mineral isochron ages of M2 clinopyroxene and garnet are 452.1 ± 7.5, 448 ± 13 and 451 ± 43 Ma (Brueckner and Van Roermund, 2007; Brueckner et al., 2004). Thus, crustal incorporation of the FGP predated that for garnet peridotite occurrences in the Western Gneiss Complex (WGC) at 430–400 Ma (Brueckner et al., 2010; Spengler, 2006; Spengler et al., 2006, 2009; Van Roermund, 2009).

4. Petrography and microstructures

This section includes a detailed description of the parageneses and microstructures of M1a–b, M2 and M3 mineral assemblages in garnet peridotite and metabasic dyke. The supplementary materials include a detailed fabric analysis of M1, M2 and M3 olivine microstructures. All mineral abbreviations are according to Whitney and Evans (2010).

4.1. The M1(a + b) assemblage

In peridotite, the M1a assemblage consists of mm- to cm-sized porphyroclasts of olivine, orthopyroxene, clinopyroxene and garnet surrounded by the finer grained M2 assemblage. All M1a porphyroclasts are heavily fractured, deformed and partially replaced by later (M2 or M3) mineral assemblages. M1a olivines are mm-sized, although in low strain domains they can reach sizes up to 1–2 cm. Most olivine porphyroclasts show undulatory extinction and kink bands (Fig. 2e). M1a orthopyroxenes and clinopyroxenes are 0.5–0.8 cm in size and often show undulatory extinction (Fig. 2a–b). Both pyroxenes show exsolution lamellae, e.g. Grt ± Spl in clinopyroxene and Grt ± Cpx in orthopyroxene. The exsolved phases are interpreted to have precipitated from the primary M1a pyroxenes during cooling and decompression between M1a and M1b (or during M1b). The exsolution microstructures indicate that M1a pyroxene mineral compositions can no longer be determined by standard EMP spot analyses, consequently a more elaborate EMP technique was used (see below). In peridotite, M1a garnet is rarely preserved (Fig. 2a–b). However, it does occur, and an example was previously presented by Brueckner et al., 2004 (Fig. 3a). More commonly, the M1a garnet–olivine assemblage is replaced by a relatively coarse-grained kelyphite (Fig. 3a–b), here called the M1b kelyphite that consists of two pyroxenes, spinel and amphibole (providing water was present). The M1b microstructure is crucial for the overall interpretation of the PTt path of the FGP body, and for this reason it is described here in detail. A good example of this M1b microstructure was first presented by Brueckner et al. (2004) and reproduced here in Fig. 3b. In this figure it is important to note that the relatively thick and dark rims around the globular spinels that surround the inner kelyphitic M1b structure (Fig. 3b) consist of a much finer grained M3 kelyphite that replaces a former M2 garnet that previously had grown around the M1b globular spinels. More frequently, such relicts of the M1b kelyphite that replaced M1a garnet are fully overgrown by the M2 assemblage consisting of (M2) Grt + Spl + Opx + Cpx-Amp (Figs. 2a–b; 3a).

As can be seen in Fig. 3a, relicts of the M1b microstructure are still present in the form of the radiating spinel stringers visible in the core of the microstructure, as well as by the coarser grained M1b spinels in the outer part of the kelyphite. The latter spinel is also compositionally zoned, as illustrated in the BSE image by the grey colour in the core, grading into white towards the rim. The same white BSE shade also characterises the radiating spinel strings inside the core of this microstructure, where the white spinel stringers co-exist with M2 garnet. The same white shade is also visible around the outer M1b spinel, where they occur in contact with M2 garnet that has grown around it. Assuming no change in volume during the M1b kelyphite-forming reaction, M1a garnet crystals were originally about 0.5–1.5 cm in size. Van Roermund (1989) and Brueckner et al. (2004) described relics of M1a garnet crystals up to 5 cm in size; most of them completely replaced by the M2 assemblage. M1a mineral phases (especially M1a olivines) are commonly heavily deformed and cross-cut by trails of mono- or multiphase solid inclusions, usually consisting of Sr-bearing Mg–Fe–Ca carbonates, diopside, Fe–Ni sulphides and rutile (Fig. 2d–e). Similar mineral phases, including a carbon phase (unidentified as yet), have recently been found in the stable M2 assemblage (Olfert, 2014 and see below). Furthermore, in garnet peridotite, the M1b stage is also interpreted to be represented by the exsolution lamellae of garnet, clinopyroxene and orthopyroxene and their host pyroxenes. Clearly, this exsolution microstructure is derived from original high-Al pyroxenes (Fig. 2a–b).

In the metabasic rocks (garnet pyroxenite, garnet websterite or eclogite), the microstructure of the M1 assemblage in low strain domains consists of large megacrysts (up to 1 cm) of Cpx + Grt ± Opx ± Fe–Ni sulphides occurring in a coarse-grained and equigranular texture (Nicolas and Poirier, 1976). The coarse-grained minerals are often heavily strained and fractured, but still have slightly curved grain boundaries meeting in triple point junctions. The M1a garnet is rarely preserved. In contrast, in high strain domains and fully recrystallized samples, the former size of M1a garnet can be inferred from the outer shape of dynamically stretched, recrystallized M2 garnet domains (Fig. 2h; Fig. 3b of Van Roermund, 1989). In the example of Fig. 2h, the two garnet generations can be inferred from the size and shape of the M1a garnet domains in comparison to the well recrystallized M2 garnet grain size. The surrounding M2 clinopyroxenes in Fig. 2h are also dynamically recrystallized and define the M2 mineral assemblage. Larger M1 clinopyroxene clasts can still be identified locally within the M2 clinopyroxene matrix. Several of these pyroxene porphyroclasts contain Opx + Grt exsolution lamellae and trails of fluid and solid inclusions that cross-cut the M1a host mineral. Due to strain partitioning effects throughout the FGP body, transitions between the two microstructural domains (M1a and M2) are common. M1b microstructures; similar to those described for the garnet peridotites are not present in metabasic rocks, except for the exsolution lamellae inside M1a pyroxene host crystals. The bulk rock composition of the crosscutting metabasic dyke is highly variable, changing from eclogite to garnet bearing websterite on the hand sample scale. Verbaas and Van Roermund (2012) found a strong positive Eu anomaly in some, but not all samples of the crosscutting (U)HP metabasic dyke. This has been interpreted to indicate the former presence of plagioclase during crystallization of the dyke within the garnet peridotite. Note: The M1b kelyphite (i.e. the breakdown of M1a garnet into spinel-bearing M1b kelyphite) does not occur in eclogite or garnet pyroxenite.

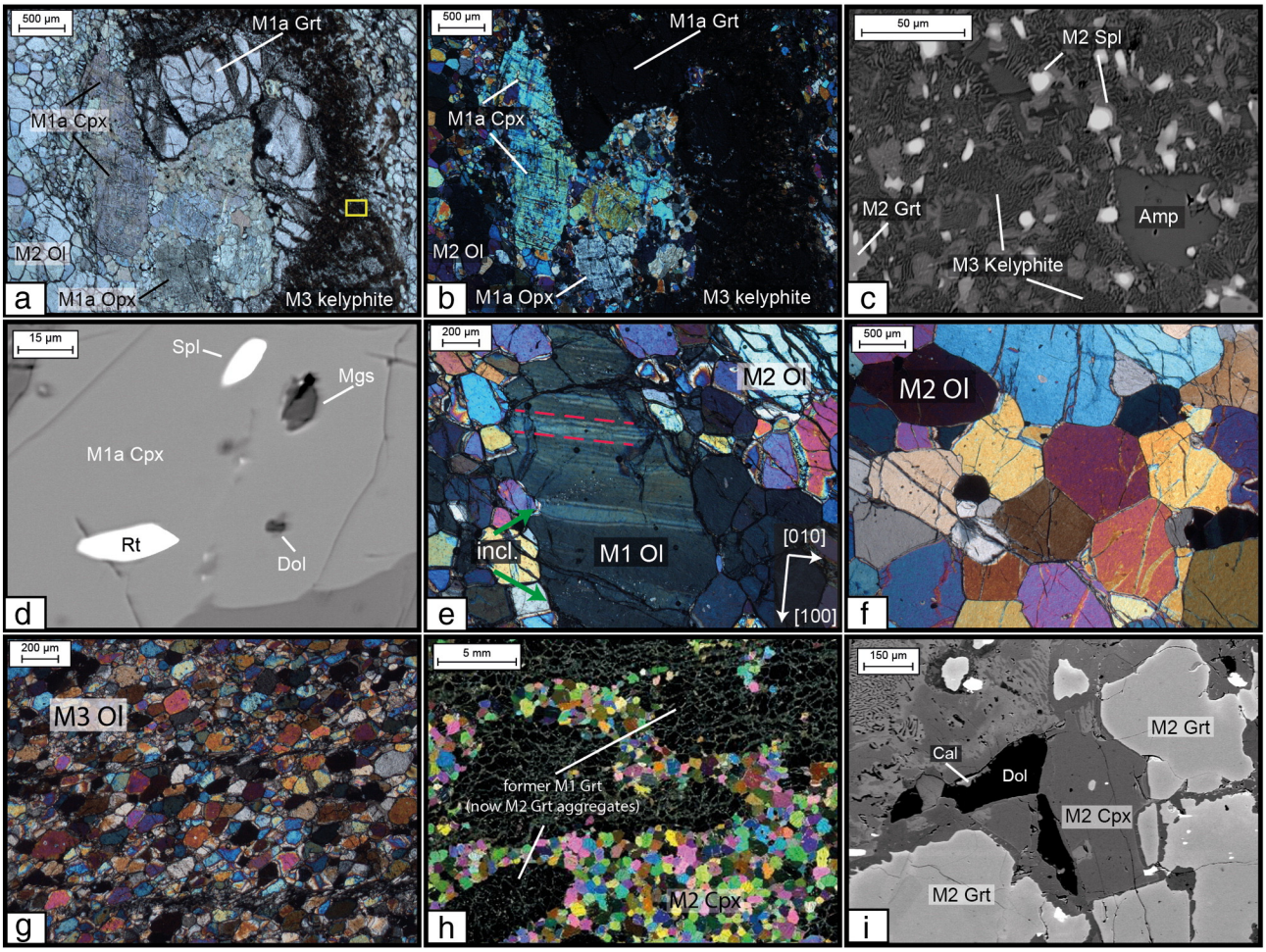

Fig. 2. Optical and electron micrographs of representative microstructures and minerals in FGP. a) PPL micrograph of M1a mineral assemblage. Note the set of fractures in M1a garnet, now filled with M2 Grt + Spl ± Amp and the characteristic M2 kelyphite replacing M1a garnet at the rims where in contact with olivine (frame magnified in Fig. 2c). b) XPL micrograph, field of view similar to a). Note garnet exsolution in clinopyroxene and orthopyroxene occurring as straight, black lines meeting at angles of about 90° (Sample F8). c) BSE image showing M3 kelyphite after M1a–b and M2 garnet (image size is the square in Fig. 2a). Note the μm-sized vermicular structure and the inverse chemical zoning (brighter to darker = Cr-rich to Al-rich from core to rim) of relict M2 spinel. d) BSE image showing spinel, rutile and carbonate inclusions inside M1a clinopyroxene (Sample F8). Carbonates (dolomite and magnesite) probably formed from the reaction between the mineral phase and COH-rich fluids, as described in Scambelluri et al. (2010). e) XPL micrograph of an M1a olivine crystal surrounded by smaller M2 olivine crystals of the "foam" microstructure. Note the set of inclined kink band boundaries parallel to the [010] direction of olivine (enlightened by dashed lines) with irregular spacing. Furthermore, note the sets of tiny white coloured inclusions cross-cutting the M1a olivine, arranged along straight lines (inclined planes) and abruptly stopping at the contact with M2 olivine "foam" crystals (Sample F8). f) XPL micrograph of the M2 olivine "foam" microstructure. Note the olivine crystals are strain free having straight boundaries meeting in triple junctions (Sample F7). g) XPL micrograph of M3 olivine "foam-like" microstructure within a D3 shear zone. Note the more tabular shaped sizes of olivine, the bimodal grain size distribution and the much smaller scale compared to Fig. 2e (Sample F10). h) XPL micrograph of M2 mineral assemblage in eclogite. Note Omphacite grains are optically strain free with straight boundaries meeting in 120^0 angles resembling the M2 olivine "foam" microstructure in f). Also note the larger M1a garnet domain sizes, now completely recrystallized into finer grained M2 garnet (Sample D51; Verbaas and Van Roermund, 2012). i) BSE image of the M2 mineral assemblage in eclogite. Note the brighter coloured outer rim of M2 garnet, indicating late stage partial re-equilibration during M3. Also note the dolomite crystal (with calcite rims) in equilibrium with garnet and omphacite.

4.2. The M2 assemblage

In garnet peridotite, the M2 stage consists of M2 Ol + Opx + Grt + Spl ± Cpx ± Amp. These M2 grains display a well-defined annealed microstructure (Fig. 2e–f), characterised by optically strain free grains having straight grain boundaries meeting in 120° triple point junctions (foam microstructure). The grain size of the foam microstructure depends on the mineral mode of each rock type, ranging from 100 μm in garnet harzburgite and lherzolite, up to 1–2 mm in dunite. In garnet peridotite, it is often possible to see the microstructural transition between M1a and M2 olivine grains. In all cases, the M1a olivine grains form larger porphyroclasts floating in a finer grained M2 olivine matrix (Fig. 2e). The M2 pyroxenes show similar microstructures except for their dynamically recrystallized grain size.

Depending on the bulk rock composition of the metabasic dikes, the M2 assemblage consists of recrystallized grains of M2 Cpx + Grt with local occurrences of zoisite, dolomite, phengite and kyanite in eclogite (Fig. 2h–i). M2 clinopyroxene is generally smaller than M1 clinopyroxene (100–200 μm in size) and commonly shows straight grain boundaries that meet in 120° triple junctions, resembling the olivine foam microstructure in peridotite (Fig. 2h). The M2 pyroxene foam microstructure is especially well developed in sodian augite, whereas omphacite generally is transformed into M3 Di + Pl symplectite. Note that this symplectitic microstructure after M2 omphacite is undeformed and in detail resembles that described by Joanny et al. (1991). The microstructure of dynamically recrystallized M2 garnets is similar to that of M2 olivine and pyroxene in which relatively straight grain boundaries meet in 120° triple junctions (Fig. 2h). However, the internal, defect-free, garnet microstructure is hard to detect due to the isotropic character of the crystals. M2 garnets occur either in clusters, completely replacing former M1a garnet domains or as smaller single grains (50–100 μm in size) in the dynamically recrystallized M2 pyroxene matrix. In BSE images all recrystallized M2 garnets (including M2 garnet "clusters" after M1a garnet) show a narrow (5–10 μm thick) and bright halo around their rims (Fig. 2i).

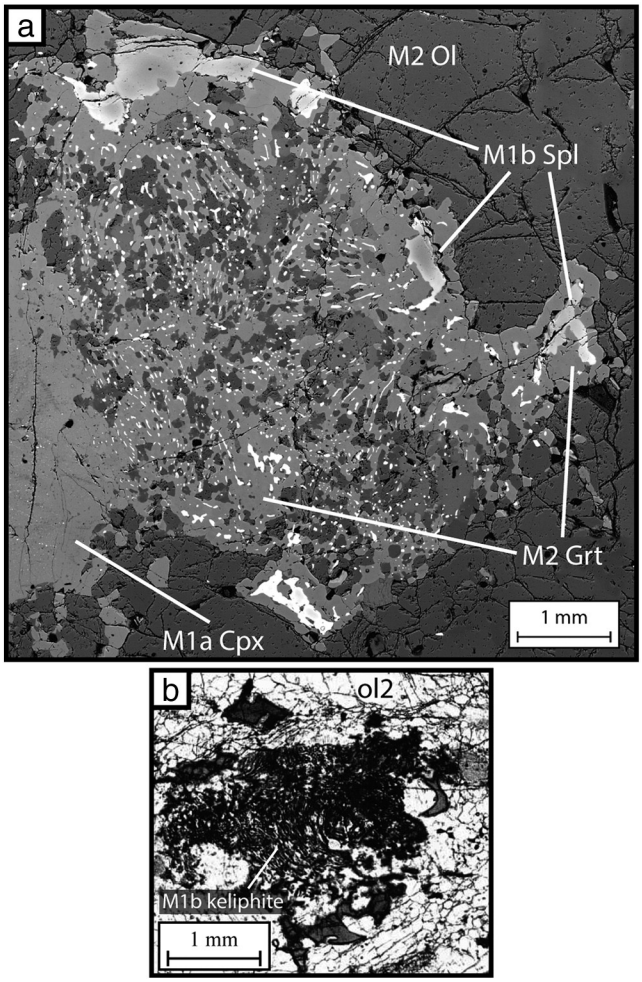

Fig. 3. a) BSE image of a M1b kelyphite, partially overprinted by the M2 assemblage including M2 garnet, orthopyroxene and amphibole. M1a clinopyroxene (to the left) and M2 olivine crystals surround the relict M1b kelyphitic microstructure. Note also the M2 garnet rims around the large globular M1b spinel. The relative temporal relationships are the following: (1) large M1a garnet is stable with M1a clinopyroxene. (2) M1a garnet + olivine breaks down in Opx + Spl + Par kelyphite. The size of spinels increases towards the rims of the kelyphite. (3) M2 mineral assemblages replace the M1b kelyphitic microstructure, only the globular spinels and the radially arranged spinel stringers remind to the original microstructure. The M2 overprint is responsible for the chemical zoning of the globular spinels. b) A similar M1b kelyphite, which largely escaped the M2 metamorphic overprint (Brueckner et al., 2004). However, note the thin dark rims around the globular spinels represent M3 kelyphites after M2 garnet (as illustrated in Fig. 2c).

4.3. The M3 assemblage

In garnet peridotite, the M3 assemblage is defined by Ol + Opx ± Amp ± Chl. This assemblage is associated with D3 deformation, which is typically restricted to anastomosing shear zones that cross-cut all earlier M1 and M2 microstructures. Relict domains of former M1 and M2 mineral assemblages are highly stretched, flattened and re-equilibrated into the M3 Opx + Amp ± Chl assemblage defining the S3 foliation. M3 microstructures developed in dunite also display a foam microstructure but the M3 olivine grains are smaller (20–80 μm), slightly tabular (Fig. 2g), and define the S3 foliation. In some inner portions of the FGP, i.e. at locations unaffected by the D3 deformation, a static overprint of M1a–b and M2 garnet–olivine mineral assemblages (especially M1a and M2 garnet) locally occur. Here, a late-stage, very fine grained kelyphite, consisting of Spl + Opx + Amp, partially or totally replaces former M1 and M2 garnets (Fig. 2a–b–c). This reaction appears optically as a brownish rim, where M1a and M2 garnets are in contact with olivine. This kelyphite can easily be distinguished from the M1b kelyphite due to its much finer lamellar spacing (thickness < 10 μm, i.e. one order of magnitude smaller; compare Figs. 2a–b–c and 3a–b). Such kelyphite formed during isothermal decompression when garnet and olivine became incompatible following the higher pressure M2 stage. We interpret such kelyphite as an M3 assemblage.

In metabasic dykes, the M3 assemblage is characterised by partial or complete breakdown of the M2 mineral phases. If clinopyroxene is more Na-rich, Ab + Di symplectite starts to form along their rims during isothermal decompression (M3), preventing recognition of the M2 foam microstructure (Fig. 2i). Omphacite, kyanite and phengite are replaced by Di + Pl and Spr + An symplectites respectively. Good examples are given by Janák et al. (2013). Dolomite grains, if present, show partial rims of calcite (Fig. 2i).

5. Mineral chemistry

In this section, the mineral chemistry of the FGP body is described as well as "reviewed" using previously published data (Brueckner et al., 2004; Van Roermund, 1989). Electron microprobe (EMP) analyses of representative minerals from spinel dunite and garnet peridotite are given in Table 1. All EMP mineral analyses presented in Table 1 are from samples F8 (garnet lherzolite) and F7 (dunite). For a description of the mineral chemistry of eclogite, the reader is referred to the recent work by Janák et al. (2013). For a description of analytical techniques, see the supplementary materials.

5.1. Olivine

In garnet peridotite (F8), no significant difference in composition is observed between M1a and M2 olivine ($Mg^{\#} = 0.905–0.925$), and results overlap with previously published data (Brueckner et al., 2004). In dunite (F7), M2 olivine is characterised by a very high Mg# (0.925–0.935; Fig. 4). NiO content in olivine (0.38–0.45) is comparable for both lithologies.

5.2. Pyroxene

Orthopyroxene is enstatite in composition. Its Mg# varies according to both lithology and PT equilibration conditions. In garnet peridotite M1a orthopyroxene has a slightly lower Mg# (=0.905–0.915) than that in M1b and M2 orthopyroxene (Mg# ~ 0.92) and orthopyroxene in dunite (Mg# = 0.925–0.930). In garnet peridotite, Al content in M1a and M1b orthopyroxene varies between 0.05 and 0.12 a.p.f.u. In contrast, Al content in M2 orthopyroxene (both in garnet peridotite and dunite) is relatively constant at around 0.05 a.p.f.u. Published data show a similar trend for Al but have rather scattered Mg# (~0.90–0.94).

There is no significant variation in composition between the two generations of clinopyroxene in peridotite and results overlap with previously published data (Brueckner et al., 2004; Van Roermund, 1989). Values of Mg# vary between 0.94 and 0.96 for both M1a and M2 clinopyroxene (Fig. 5b). Al values (a.p.f.u.) range from 0.10 to 0.25 in M1a clinopyroxene while being relatively constant (~0.10) in M2 clinopyroxene. Garnet clinopyroxenite reported by Van Roermund (1989) shows Al (a.p.f.u.) values as low as 0.05. Precursor M1a clinopyroxene has Al (a.p.f.u.) values comparable with some high-Al analyses on M1a clinopyroxene (0.18–0.25 atoms p.f.u.) but show a lower Mg# (0.92–0.93). In eclogite, omphacite has generally lower Mg# (0.91–0.92) and high Al content (0.35–0.40 a.p.f.u.).

The bulk compositions of exsolved M1a ortho- and clinopyroxene were analysed using wide beam EMP analysis (beam diameter 10 μm). In order to apply this technique, well preserved areas of M1a clinopyroxene and orthopyroxene grains were selected in samples GP3 (this latter sample was chosen because it is similar in bulk rock composition and microstructure to those in sample F8) and four line scans of 30 points were performed ($4.32 \times 10–5\ mm^3$). Results are listed in Table 2.

Table 1
Representative EMP analyses of mineral compositions in garnet peridotite and dunite from the FGP.

Mineral	Olivine						Orthopyroxene							
Lithology	Dunite (F7)		Garnet peridotite (F8)				Dunite (F7)		Garnet peridotite (F8)					
Mineral assemblage	M2 "foam" microstructure		M1a porphyroclasts		M2 "foam" microstructure		M2		M1a porphyroclasts		M1b kelyphite after M2 "foam" M1a Grt		M2 "foam" microstructure	
SiO2	40.75	40.82	40.16	40.10	40.29	40.25	57.39	57.30	56.62	56.77	56.68	56.70	57.39	57.37
TiO2	–	–	–	–	–	–	0.00	0.01	0.10	0.07	0.07	0.07	0.04	0.05
Al2O3	–	–	–	–	–	–	1.27	1.16	1.15	1.17	1.46	1.61	1.17	1.03
Cr2O3	0.01	0.02	0.00	0.00	0.02	0.00	0.38	0.33	0.19	0.18	0.19	0.26	0.53	0.53
FeO	7.37	7.27	9.21	9.24	9.28	9.23	5.07	5.17	5.91	6.36	5.52	5.43	5.01	5.44
MnO	0.09	0.08	0.10	0.10	0.08	0.08	0.12	0.13	0.11	0.11	0.08	0.06	0.11	0.18
MgO	50.12	50.20	49.67	49.37	49.17	49.24	35.25	35.55	34.86	34.31	34.54	35.05	35.49	35.63
NiO	0.39	0.43	0.38	0.39	0.37	0.40	–	–	–	–	–	–	–	–
CaO	0.00	0.00	0.00	0.00	0.00	0.00	0.20	0.17	0.19	0.17	0.16	0.15	0.17	0.20
Na2O	–	–	–	–	–	–	0.00	0.05	0.00	0.00	0.03	0.00	0.00	0.02
TOTAL	98.73	98.82	99.52	99.20	99.21	99.20	99.68	99.87	99.13	99.14	98.73	99.33	99.91	100.12
Al (p.f.u.)	–	–	–	–	–	–	0.051	0.047	0.047	0.048	0.060	0.066	0.047	0.042
Mg#	0.924	0.925	0.917	0.905	0.912	0.913	0.925	0.925	0.913	0.906	0.918	0.920	0.927	0.921
Cr#	–	–	–	–	–	–	–	–	–	–	–	–	–	–

Mineral	Clinopyroxene				Garnet									
Lithology	Garnet peridotite (F8)				Garnet peridotite (F8)									
Mineral assemblage	M1a porphyroclasts		M2 "foam" microstructure		M1a		M2		M2 (in M1b Spl rims)		M2 (Opx exsol. lamellae)		M2 (Cpx exsol. lamellae)	
SiO2	54.16	53.60	54.25	54.20	41.86	41.54	41.94	41.88	41.41	40.79	42.01	41.21	41.45	41.74
TiO2	0.22	0.20	0.14	0.15	0.06	0.10	0.02	0.03	0.04	0.06	0.02	0.03	0.05	0.06
Al2O3	2.30	2.15	2.23	2.23	21.67	21.79	22.53	22.82	22.83	22.37	22.67	22.44	22.02	22.24
Cr2O3	1.16	1.04	0.77	0.67	2.20	2.13	1.02	0.99	1.01	1.01	1.09	1.11	1.38	1.32
FeO	1.63	1.61	1.61	1.78	9.82	9.89	10.39	10.24	9.30	9.70	10.81	10.94	12.04	11.81
MnO	0.06	0.04	0.04	0.03	0.44	0.47	0.45	0.45	0.54	0.59	0.59	0.68	0.81	0.90
MgO	16.11	16.26	16.19	16.30	18.70	18.77	18.64	19.02	19.36	18.68	18.62	18.54	16.97	16.74
NiO	0.01	0.00	–	–	0.00	0.00	0.00	0.00	0.02	0.06	0.00	0.00	0.04	0.00
CaO	22.77	22.83	22.63	22.65	5.13	5.01	4.53	4.40	4.81	4.66	4.44	4.09	5.24	5.34
Na2O	1.23	1.12	1.30	1.27	–	–	–	–	–	–	–	–	–	–
TOTAL	99.65	98.85	99.16	99.28	99.88	99.70	99.52	99.83	99.32	97.92	100.25	99.04	100.00	100.15
Al (p.f.u.)	0.098	0.093	0.096	0.096	–	–	–	–	–	–	–	–	–	–
Mg#	0.946	0.947	0.947	0.942	0.670[a]	0.672[a]	0.672[a]	0.681[a]	0.691[a]	0.680[a]	0.668[a]	0.671[a]	0.617[a]	0.615[a]
Cr#	–	–	–	–	0.064	0.062	0.029	0.028	0.029	0.029	0.031	0.032	0.040	0.038

Mineral	Spinel								Amphibole			
Lithology	Dunite (F7)		Garnet peridotite (F8)						Garnet peridotite (F8)			
Mineral assemblage M2	M2		M1b (core)		M1b (rim)		M2		M2			
SiO2	0.01	0.02	0.01	0.02	0.00	0.03	0.32	0.26	43.69	43.14	44.34	44.34
TiO2	0.02	0.04	0.03	0.02	0.04	0.03	0.01	0.04	1.20	0.94	0.99	1.09
Al2O3	30.10	29.06	52.50	52.28	46.28	45.39	46.24	42.30	14.70	13.36	12.84	12.78
Cr2O3	38.03	39.30	16.96	16.88	23.20	23.95	22.01	25.68	1.92	1.50	1.75	1.75
FeO	16.16	16.23	9.32	9.52	11.26	11.30	11.28	11.87	2.17	3.44	2.78	2.90
MnO	0.58	0.61	0.25	0.25	0.33	0.31	0.27	0.33	0.00	0.09	0.00	0.05
MgO	14.40	14.23	20.70	20.61	18.97	18.89	19.35	18.06	16.98	17.05	18.35	18.22
NiO	0.03	0.09	0.24	0.25	0.18	0.19	0.05	0.06	–	–	–	–
CaO	–	–	–	–	–	–	–	–	11.90	12.19	12.06	12.13
Na2O	–	–	–	–	–	–	–	–	2.61	2.62	3.16	3.05
K2O	–	–	–	–	–	–	–	–	0.02	0.03	0.00	0.00
ZnO	0.26	0.28	0.33	0.38	0.23	0.31	0.24	0.19	–	–	–	–
VO	0.26	0.20	0.14	0.17	0.18	0.20	0.09	0.13	–	–	–	–
TOTAL	99.85	100.06	100.48	100.38	100.67	100.60	99.86	98.92	95.19	94.36	96.27	96.31
Al (p.f.u.)	–	–	–	–	–	–	–	–	–	–		
Mg#	0.614	0.610	0.798	0.794	0.750	0.749	0.754	0.731	0.933	0.919	0.955	0.978
Cr#	0.459	0.476	0.178	0.178	0.252	0.261	0.242	0.289	–	–	–	–

[a] Mg# in garnet is calculated as Mg/(Fe + Mg + Ca).

The M1a orthopyroxene and M1a clinopyroxene precursors show higher Al (p.f.u.) contents (up to 0.2 atoms p.f.u.) and lower Mg# when compared to other M2 pyroxene compositions (Fig. 5a–b).

5.3. Spinel

In garnet peridotite (sample F8) two spinel compositions occur (designated M1b and M2). The M1b type is represented by the large (0.5–2 mm) globular spinel (Cr# = 0.16–0.23; Mg# = 0.78–0.86) found around M1b kelyphites after M1a garnet (Fig. 3a). The chemical zoning in the globular spinel is represented by a relative increase in Cr# and concomitant decrease in Mg# towards the rims (Fig. 6a). The spinel rim composition in direct contact with M2 garnet (Figs. 3a and 6b) is interpreted as that of M2 spinel (Cr# = 0.21–0.42; Mg# = 0.61–0.80). Consequently, the globular spinel core composition is interpreted as a relict M1b composition.

In Al-poor dunite (sample F7) spinel is chemically unzoned and usually associated with M2 orthopyroxene in clusters. M2 spinel in dunite

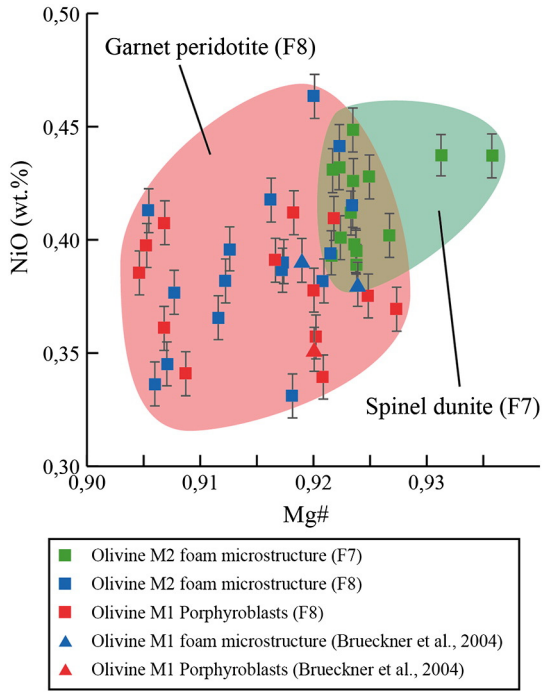

Fig. 4. Diagram illustrating NiO (wt.%) VS Mg# of olivine in different textures and rock types.

Table 2
Results of chemical integration using defocussed EMP mapping on M1a orthopyroxene and clinopyroxene.

	WBA	
	opx	cpx
SiO2	55.63	50.32
TiO2	0.07	0.37
Al2O3	2.25	4.9
Cr2O3	0.39	1.36
FeO	6.09	2.64
MnO	0.11	0.1
MgO	34.24	16.5
NiO	0.08	0.05
CaO	0.42	20.02
Na2O	0.06	1.15
Total	99.34	97.41
Si	1.934	1.876
Ti	0.002	0.01
Al	0.092	0.215
Cr	0.011	0.04
Fe	0.177	0.082
Mn	0.003	0.003
Mg	1.774	0.917
Ni	0.002	0.001
Ca	0.016	0.8
Na	0.004	0.083
Total	4.015	4.028
Mg#	0.909	0.918
Cr#	0.107	0.157

has the most Cr-rich and Mg-poor composition among the investigated samples, with a Cr# of 0.46–0.51 and Mg# of 0.61–0.66 (Fig. 6a).

5.4. Garnet

In garnet peridotite (F8), M1a and M2 garnets have different mineral compositions. M1a garnet is relatively Cr-rich, with Cr_2O_3 values between 1.80–2.3 wt.% (Cr# ~0.060–0.065), in contrast to M2 garnet which has Cr_2O_3 values ranging between 0.50–1.5 wt.% (Cr# ~0.027–0.033; Fig. 7b; Table 1). Note that the low Cr# M2 garnet is always associated with high Cr# (M2) spinel. In contrast, spinel is absent in the primary M1a assemblage. M1a garnet has a composition of pyrope ~70–76%, almandine + spessartine ~18–21% and grossular + andradite ~6–10% (Fig. 7a), comparable to that reported by Brueckner et al. (2004).

Exsolved garnet lamellae within M1a orthopyroxene have approximately the same composition as that of M2 garnet, and exsolved garnet lamellae within M1a clinopyroxene show a slightly lower pyrope content (Fig. 7a). In both cases, the Cr# is ~0.03.

M2 garnet has generally the same composition as that of M1a garnet in terms of pyrope and almandine + spessartine contents, although its grossular content increases to around 9–12% and its Cr# decreases to around 0.03 (Fig. 7a).

5.5. Amphibole

All analysed amphiboles are pargasite in composition (Table 1), according to the classification of Leake et al. (1997). They are similar in composition to amphiboles reported by Van Roermund (1989) and Brueckner et al. (2004).

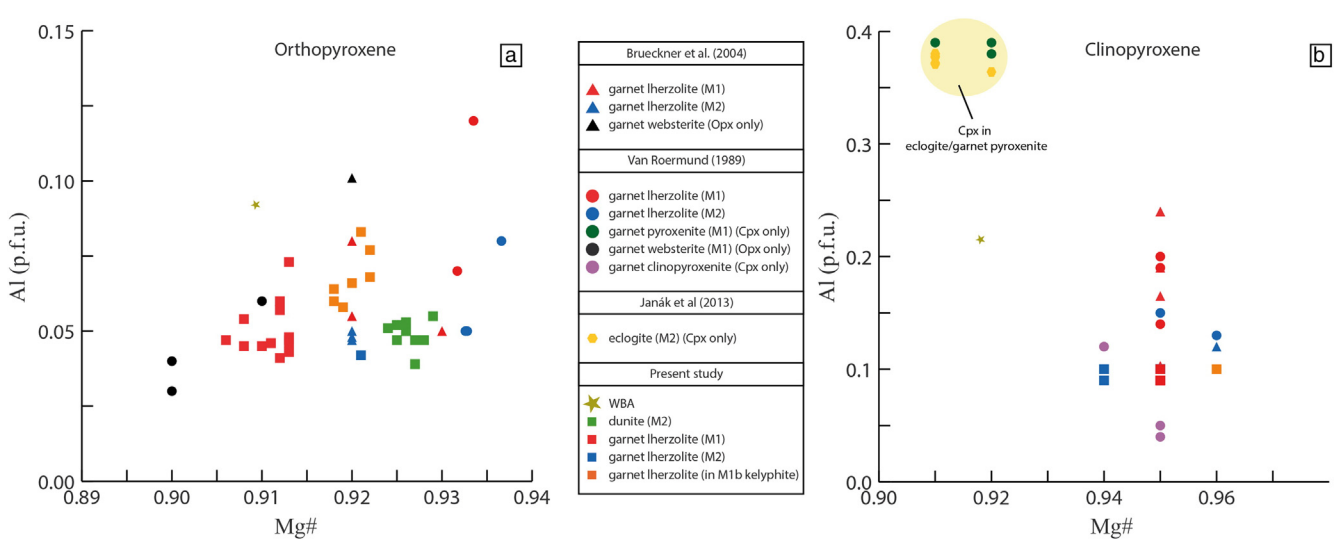

Fig. 5. Diagram illustrating Al (p.f.u.) VS Mg# of orthopyroxene (a) and clinopyroxene (b) in different textures and rock types.

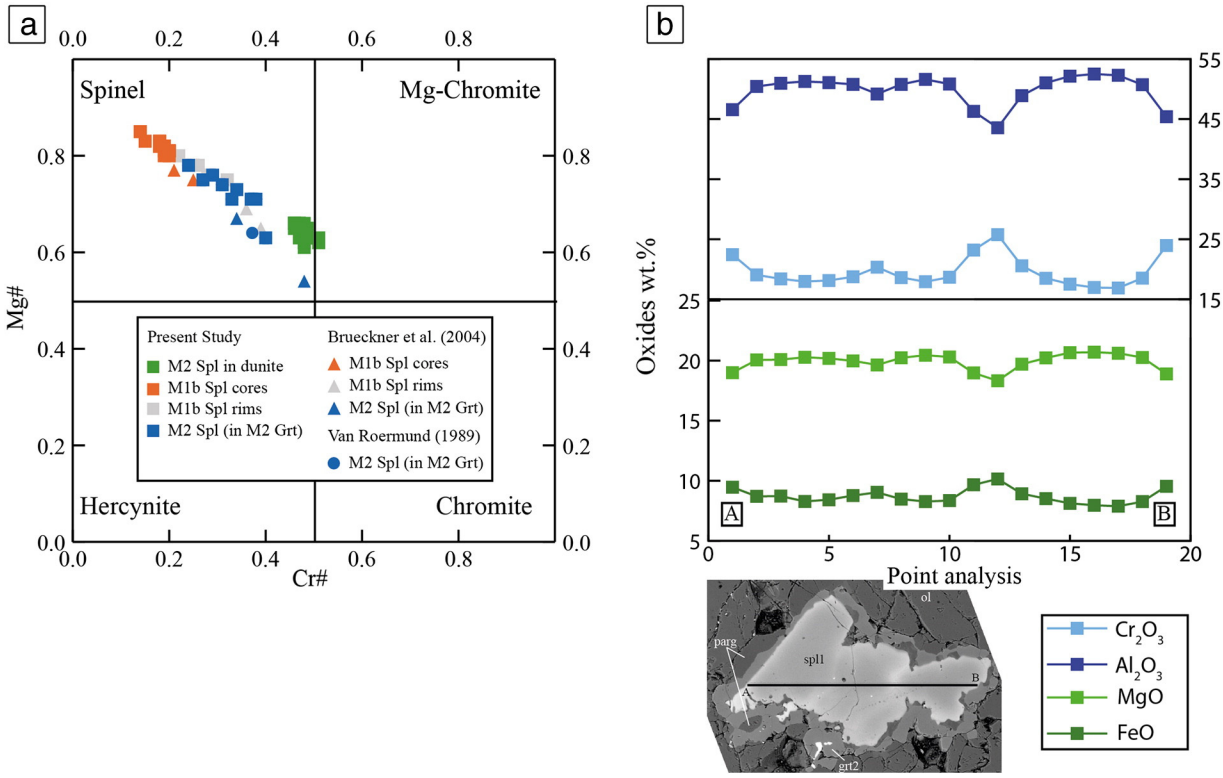

Fig. 6. a) Diagram illustrating Mg# VS Cr# in different generations of spinel from different bulk rock compositions. b) EMP line-scan AB (450 μm) across a zoned, globular, M1b spinel. At the rims, in contact with M2 garnet and Pargasite, Al and Mg content decreases, and Fe and Cr content increases.

6. PT conditions

6.1. Results of geothermobarometry

We have calculated the PT conditions of metamorphic stages recognised in the FGP using various geothermobarometric techniques in combination with EMP mineral and wide beam analyses (WBA) listed in Tables 1 and 2. Calculated PT results are summarised in Fig. 8 and Table **3**. For a review of the selected geothermobarometers, the reader is referred to Krogh-Ravna and Paquin (2003) and Brey et al. (2008).

6.1.1. M1a conditions

According to Brenker and Brey (1997), the preferred way to calculate temperature for garnet peridotite is to use the Fe–Mg exchange thermometer between olivine and garnet (O'Neill, 1980; O'Neill and Wood, 1979; Wu and Zhao, 2007), because garnet is a slow diffusing phase (Carlson, 2006) and the composition of olivine remains relatively constant in olivine-rich bulk compositions (>75 modal %). Temperatures derived in such a way can then be combined with the Al content of orthopyroxene (P_{BKN90}; P_{NG85}) to obtain a pressure estimate, provided that the composition of orthopyroxene is in equilibrium with that of garnet. Fig. 8a (M1a) shows that for M1a garnet and olivine, T_{WZ07} intersects P_{BKN90} and P_{NG85} at T slightly above and P slightly below the M2 PT conditions, which were independently derived by Janák et al. (2013) using an alternative geothermobarometric technique.

6.1.2. M1b conditions

The Fe–Mg exchange thermometers between Ol and Spl (T_{Bal91} of Ballhaus et al., 1991 and T_{OW87} of O'Neill and Wall, 1987) were applied to M1b spinel core and rim compositions to estimate M1b equilibrium temperatures (Table 3). The influence of Fe^{3+}/Fe^{2+} ratios on the various thermometers is taken to be negligible. For this calculation, we took a M1b spinel core composition with an exceptionally low (in the core) and high (at the rim) Cr amount (Table 1). For a pre-set P of 1.4 GPa (pressure estimate of the M1b mineral assemblage based on the Spl–Grt transition line in the pseudosection of Fig. 11) T_{Bal91} gives 890 ± 20 °C for the spinel core and 790 ± 20 °C for the spinel rim. T_{OW98} gives slightly lower temperatures of about 840 ± 20 °C for the spinel core and 770 ± 20 °C for the spinel rim.

6.1.3. M2 conditions

We used representative EMP mineral analyses (Table 1) from garnet peridotite (F8) and dunite (F7) to calculate M2 equilibrium conditions (Table 3) using the experimentally calibrated geothermobarometers reviewed by Krogh-Ravna and Paquin (2003) and Brey et al. (2008). The pre-set PT conditions of the M2 stage are at 800 °C and 3.0 GPa, representing the mean values calculated by Janák et al. (2013). Results are illustrated in Fig. 8c and Table 3.

Fig. 8c (M2) shows that for M2 garnet and olivine, T_{WZ07} intersect with P_{BK90} at slightly higher P with respect to the M2 derived by Janák et al. (2013). The geothermometer applied on M2 spinel $T_{Ballhaus91}$ is consistent with the M2 PT field derived by Janák et al. (2013).

6.2. Thermodynamic modelling

Pseudosections (isochemical phase diagrams in PT space) were calculated using Perple_X 6.6.8 thermodynamic software (Connolly, 2005: version 6.6.8), coupled with the latest available version of the internally consistent thermodynamic dataset of Holland and Powell (1998) upgraded for Cr-bearing phases (cr_hp02ver.dat) and modified according to Ziberna et al. (2013). Solid solution models for garnet (Mattioli and Bishop, 1984; Ziberna et al., 2013), spinel (Klemme, 2010), olivine, orthopyroxene, clinopyroxene (Holland and Powell, 1996), chlorite (Holland and Powell, 1998), eskolaite (Chatterjee et al., 1982), feldspar (Benisek et al., 2010) and amphibole (Dale et al., 2000) were used, as available from the Perple_X datafile (solution_model_666.dat) and modified according to Ziberna et al. (2013).

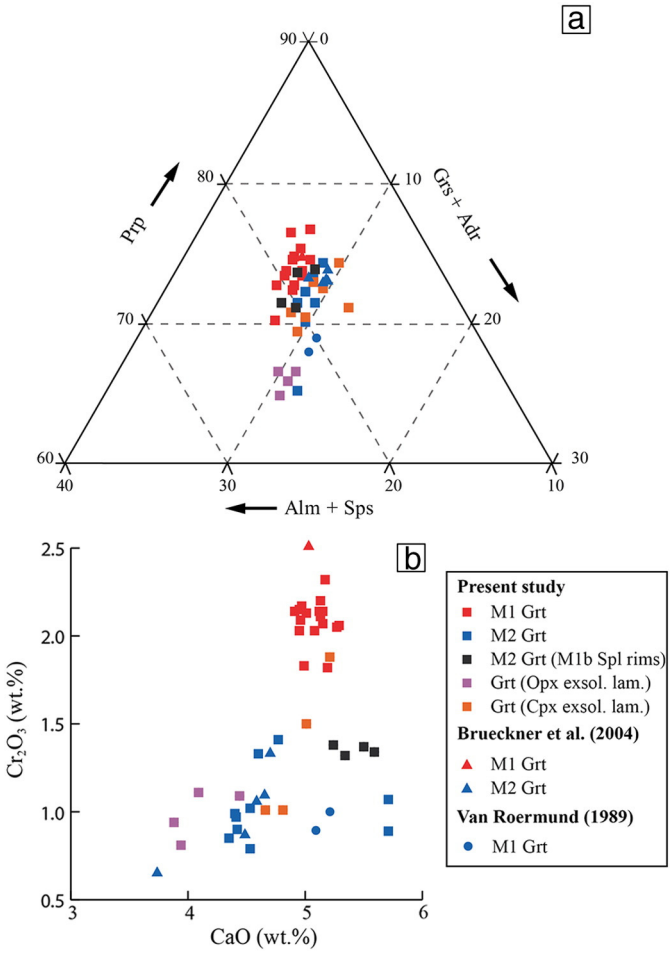

Fig. 7. a) Garnet end-member diagram. All garnets show a similar Fe/Mg ratio, however M1 garnets have a slightly lower Ca content. This garnet triplot does not include Cr-bearing end-members. b) Diagram illustrating CaO VS Cr2O3 (wt.%) in different garnet generations showing the characteristic "high-Cr" content of M1a versus to the low-Cr content of M2 garnet.

A pseudosection (Fig. 10) has been calculated for garnet lherzolite F8 between 1.0–7.0 GPa and 700–1500 °C, for the anhydrous Cr_2O_3–Na_2O–CaO–K_2O–FeO–MgO–Al_2O_3–SiO_2 (Cr-NCKFMAS) system. The XRF analysis of sample F8 is listed in the top of Fig. 10. Mn and Fe^{3+} were not included in the calculation, because the Mn content of the bulk rock composition is negligible and the Fe^{3+} content, which was not measured, is thought to be negligible also. In addition, the isopleths of Mg# = prp = [Mg/(Mg + Fe + Ca)], Ca# = grs = [Ca/(Mg + Fe + Ca)] and Cr# [Cr/(Al + Cr)] in garnet and Al (p.f.u.) in orthopyroxene were calculated and added to the figure (Fig. 10).

The star symbol in Fig. 10 indicates the PT conditions for M2, calculated by Janák et al. (2013). The shaded ellipse represents the PT conditions where M1a garnet was stable (5.0 ± 0.5 GPa–1100 ± 100 °C) and is derived using the intersection points between isopleth lines that correspond to the Mg#, Ca#, and Cr# values in M1a garnet listed in Table 1. The details of the results of the pseudosection calculations are given in the repository, a summary of the most important results are given in Fig. 10.

A second pseudosection to illustrate the M1b–M2–M3 metamorphic evolution of garnet lherzolite F8 has been calculated between 2.0–4.0 GPa and 700–1300 °C, for the Cr_2O_3–Na_2O–CaO–K_2O–FeO–MgO–Al_2O_3–SiO_2–H_2O (Cr-NCKFMASH) system, taking the activity of H_2O = 1.0 (Fig. 11). The F8 bulk rock composition is again listed in the top of the figure.

The isopleths Cr# in garnet [Cr/(Al + Cr)] and Al (p.f.u.) in clinopyroxene were calculated and added to the figure (Fig. 11). The two star symbols in Fig. 11 indicate the PT conditions for M2 and M3 as calculated by Janák et al. (2013). Within this pseudosection we have added also two shaded squares (called M1b and M2) that represent metamorphic stages experienced by the FGP: (1) the PT field of the inferred M1b mineral assemblage (1.4 ± 0.2 GPa and 850–900 °C; Fig. 8c), derived by the intersection between the temperature lines, obtained by applying T_{Bal91} and T_{OW87} to olivine and M1b spinel (core) and the Spl = Spl + Grt reaction line in Fig. 11. (2) The PT field of the M2 mineral assemblage (2.9 ± 0.1 GPa–800 ± 50 °C) derived using the Cr# in M2 garnet and Al(p.f.u.) values for M2 clinopyroxene (Table 1) in combination with the thermobarometric results derived from the M2 mineral assemblage (Fig. 8c; Table 3).

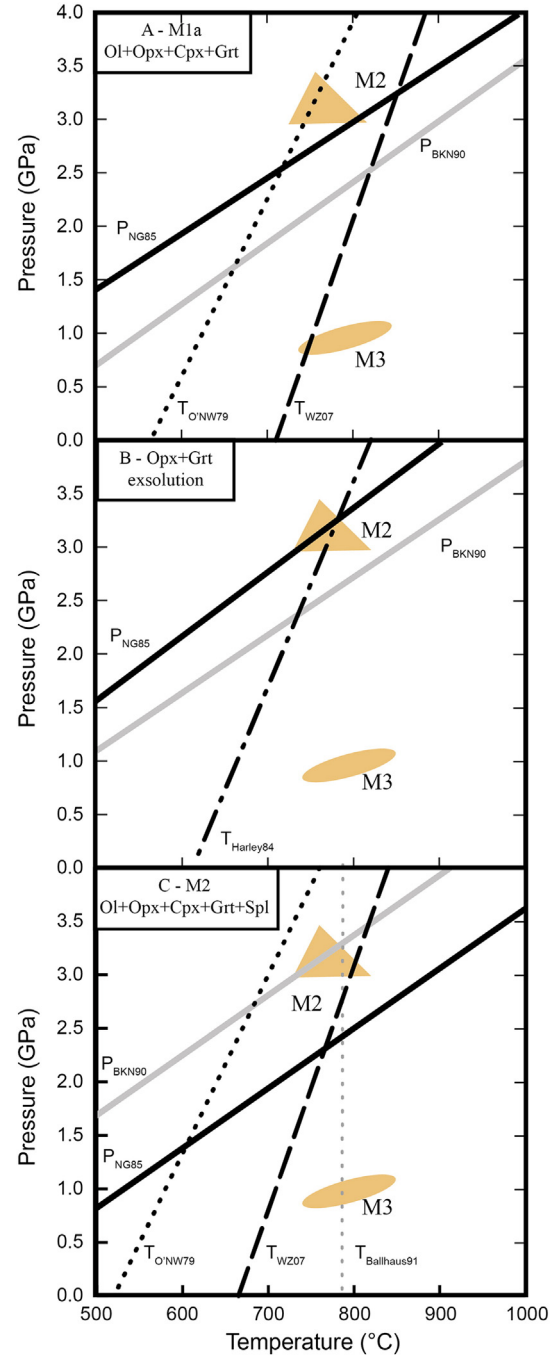

Fig. 8. Results of geothermobarometric calculations using normal EMP spot analyses performed on: a) M1a mineral assemblage, b) M1b Opx + Grt exsolution and c) M2 mineral assemblages. Positions of M2 and M3 fields according to Janák et al. (2013).

Table 3
List of used geothermobarometers for the M1a, M1b and M2 mineral assemblage from garnet lherzolite and M2 mineral assemblage from dunite.

Name	Type[b]	Preset: 975 °C/2.3 GPa	Preset: 800 °C/3.0 GPa				Preset: 1.4 GPa[a]	Reference
		WBA	M1a (F8)	M2 (F8)	M2 (dunite)	M1b Spl rim	M1b Spl core	
T [BKN90]	Opx-Cpx 'solvus'	1043 °C	620 ± 45 °C	625 ± 55 °C				Brey and Köhler (1990)
T [Krogh88]	Fe–Mg between Cpx and Grt		685 ± 10 °C	665 ± 15 °C				Krogh (1988)
T[KroghRavna00]	Fe–Mg between Grt and Cpx		640 ± 10 °C	630 ± 15 °C				Krogh-Ravna (2000)
T [O'NW79]	Fe–Mg between Ol and Grt		755 ± 5 °C	715 ± 15 °C				O'Neill and Wood (1979)
T [Harley84]	Fe–Mg between Opx and Grt		755 ± 5 °C	755 ± 15 °C				Harley (1984)
T [WZ07]	Fe–Mg between Ol and Grt		825 ± 20 °C	795 ± 20 °C				Wu and Zhao (2007)
T [EG79]	Fe–Mg between Cpx and Grt		775 ± 10 °C	760 ± 10 °C				Ellis and Green (1979)
T [Powell85]	Fe–Mg between Cpx and Grt		750 ± 10 °C	735 ± 10 °C				Powell (1985)
T [BM85]	Opx–Cpx 'solvus'	996 °C	650 ± 30 °C	695 ± 90 °C				Bertrand and Merrier (1985)
T [OpxBK90]	Single Opx	899 °C	780 ± 35 °C	780 ± 10 °C				Brey and Köhler (1990)
T [OW87]	Fe–Mg between Ol and Spl			800 ± 20 °C	645 ± 10 °C	825 ± 10 °C	850 ± 10 °C	O'Neill and Wall (1987)
T [WS91]	Al in Opx for Spl peridotites			755 ± 30 °C	810 ± 10 °C			Witt-Eickschen and Seck (1991)
T [Berman95]	Fe–Mg between Cpx and Grt		645 ± 10 °C	630 ± 15 °C				Berman et al. (1995)
T [BermanMod]	Fe–Mg between Cpx and Grt		675 ± 10 °C	670 ± 15 °C				Nakamura and Hirajima (2005)
T [Ballhaus91]	Fe–Mg between Ol and Spl			805 ± 15 °C	620 ± 10 °C	820 ± 15 °C	900 ± 10 °C	Ballhaus et al. (1991)
T [Taylor98]	Opx–Cpx 'solvus'	1189 °C	825 ± 40 °C	820 ± 50 °C				Taylor (1998)
T[NimisTaylor00]	Single Cpx		600 ± 40 °C	590 ± 55 °C				Nimis and Taylor (2000)
P[BKN90]	Al in Opx		2.3 ± 0.2 GPa	2.8 ± 0.2 GPa				Brey and Köhler (1990)
P[BBG08]	Al in Opx		2.0 ± 0.2 GPa	2.5 ± 0.2 GPa				Brey et al. (2008)
P[NG85]	Al in Opx		2.6 ± 0.2 GPa	2.9 ± 0.1 GPa				Nickel and Green (1985)
P[MC74]	Al in Opx		2.8 ± 0.2 GPa	2.8 ± 0.2 GPa				MacGregor (1974)
P[NimisTaylor00]	Single Cpx	2.2 GPa	2.9 ± 0.1 GPa	2.9 ± 0.1 GPa				Nimis and Taylor (2000)
P[RGP96]	Cr in Grt		2.7 ± 0.2 GPa	2.0 ± 0.2 GPa				Ryan et al. (1996)

[a] Preset of 1.4 GPa according to Spl = Grt + Spl transition line obtained through thermodynamic modelling.
[b] All iron is considered as Fe^{2+}, except for T [WS91] and T [Ballhaus91].

7. Discussion

7.1. PT evolution of FGP

7.1.1. Pre-M1a

The early history of the FGP is related to the formation and subsequent thermal evolution of the lithospheric mantle. Brueckner et al. (2004) suggested an Archean (~3.0 Ga) melting event, recorded by Re–Os dating of pentlandites, leading to the production of a strongly depleted mantle. Brueckner et al. (2002) and Beyer et al. (2006) suggested that a similar process plus dyke intrusions occurred within several peridotite bodies of the WGR. After melt depletion, a series of Proterozoic (1.4–1.8 Ga) refertilization events occurred, as indicated by several intrusions of basic dykes (Brueckner et al., 2010; Spengler et al., 2009). These events are thought to have reintroduced non-refractory elements like Si, Al and Ca into previously depleted mantle. Spengler et al. (2006) suggested that highly refractory dunites might accrete to the base of the cratonic lithosphere (100–150 km) during or after upwelling of relatively fertile asthenosphere that had undergone large degrees of dry decompression melting. During the mid to late Proterozoic, partial melting events occurring within the asthenosphere underneath deeper parts of this cratonic lithosphere generated basic dyke swarms (now metamorphosed). These swarms, during upward migration into the overlying cold, old and depleted cratonic lithospheric mantle, "refertilized" the overlying dunite and harzburgite of the lithospheric mantle.

7.1.2. M1a

The oldest mineral assemblage (M1a) in the garnet peridotite, Ol + Opx + Cpx + Grt, represents the remnants of the original lithospheric mantle. Thermodynamic calculations (Fig. 10) indicate that the M1a garnet (Mg# ~ 0.67, Ca# ~ 0.13 and Cr# ~ 0.065) was equilibrated at around 5.0 ± 0.5 GPa and 1100 ± 100 °C which are regarded as the PT conditions under which the M1a assemblage of FGP was formed.

The compositions of M1a and M2 garnets are strikingly similar, except for their Cr and Ca contents (Fig. 7; Table 1). Moreover, thermobarometric calculations applied to M1a olivine and M1a garnet give PT results very close to the M2 conditions (Fig. 8a). At first glance this may indicate a complete reset of the M1a mineral compositions due to extensive solid state diffusion related to the intense early Caledonian M2 metamorphic overprint (Fig. 9). However it is clear from the Mg# and Ca# isopleths in the pseudosection of Fig. 10 and the thermobarometric results presented in Table 3 that the mineral chemistry of M1a garnet has not been extensively re-equilibrated by M2 metamorphism, although M1a garnet and pyroxene mineral compositions were modified in their Ca, Cr and Al contents. However we interpret these results as follows: conventional geothermobarometry (applied to similar mineral-chemistries) will yield spurious results for the M1a assemblages, consequently conventional geothermobarometric techniques applied to M1a mineral assemblages produces inappropriate PT results. It is therefore essential, besides classic geothermobarometry, to perform additional pseudosection work as was done in the present paper. We predict that in all such cases the metamorphic temperatures of the M1a conditions will be 100–200 °C higher, while calculated P conditions had to be upgraded accordingly. This interpretation can also explain why earlier researchers always found approximately similar PT conditions for the M1(a) and M2 metamorphic events within the FGP (Brueckner et al., 2004; Van Roermund, 1989; Verbaas and Van Roermund, 2012).M1b

The partial or complete recrystallization of M1a garnet into Opx + Cpx + Spl of the M1b mineral assemblage indicates that the rocks underwent a decompressional phase while still being in the mantle. The presence of amphibole in the M1b assemblage reflects the introduction of fluids, possibly between M1a and M1b. Alternatively the amphibole could have been introduced during the severe M2 metamorphic overprint. This remains uncertain as M1b and M2 amphiboles do not show any difference in chemical composition.

According to geothermometric calculations, the M1b mineral assemblage equilibrated at 850–900 °C (Table 3). Fe–Mg exchange between olivine and M1b spinel rims indicates lower temperatures of 790 ± 20 °C (Fig. 8b4). The intersection points between the Spl = Spl + Grt

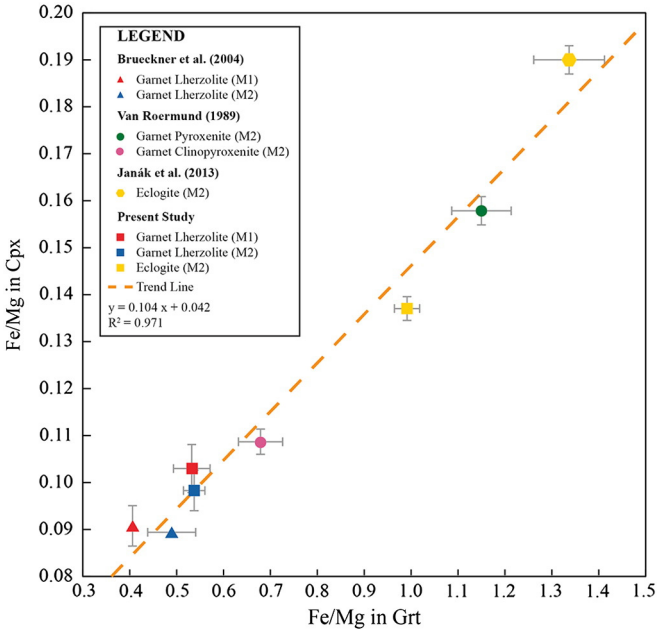

Fig. 9. Diagram illustrating the Fe/Mg (in garnet) VS Fe/Mg (in clinopyroxene) ratios in different rock types as measured by the different authors listed in the legend.

phase boundary line in Fig. 11 and the above geothermometric results define the (maximum) pressure and temperature conditions during M1b around 850–900 °C and ≤1.5 GPa. The M1b PT regime is interpreted as a progressive post M1a decompression event caused by asymmetric, large scale, lithospheric extension, most likely related to the formation of the Iapetus Ocean (Fig. 12a). During this decompression event, the extremely slow Fe–Mg diffusion rate in garnet at T < 1200 °C (Carlson, 2006) allowed the M1a garnet to maintain its original major element composition.

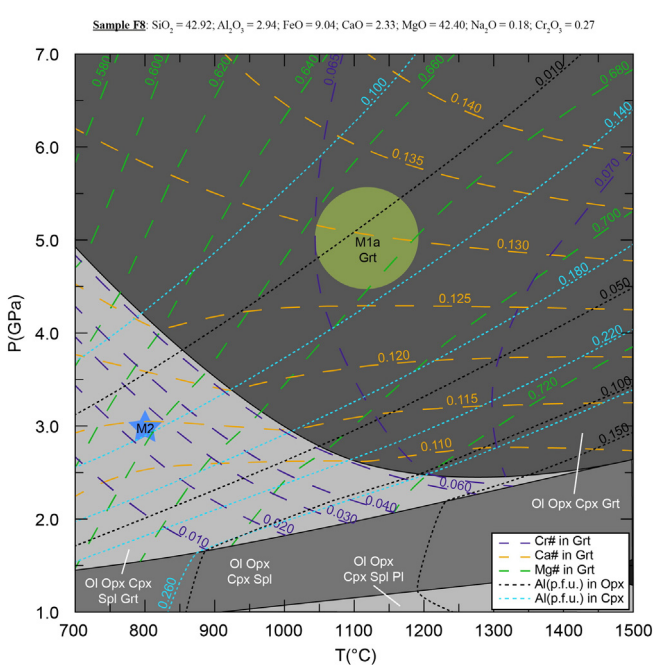

Fig. 10. PT section calculated using the Perple_X thermodynamic software (Connolly, 2005: version 6.6.8) with isopleths for Mg# = prp = (Mg/(Mg + Fe + Ca)), Ca# = grs = (Ca/(Mg + Fe + Ca)) and Cr# (Cr/(Al + Cr)) in garnet and Al (p.f.u.) content in orthopyroxene. M1a mineral assemblage in the Cr-NCFMAS system. The shaded ellipse indicates the provenance of M1a garnet (Table 1) according to mineral data and isopleths modelling. The star symbol indicates the M2 conditions of Janák et al. (2013).

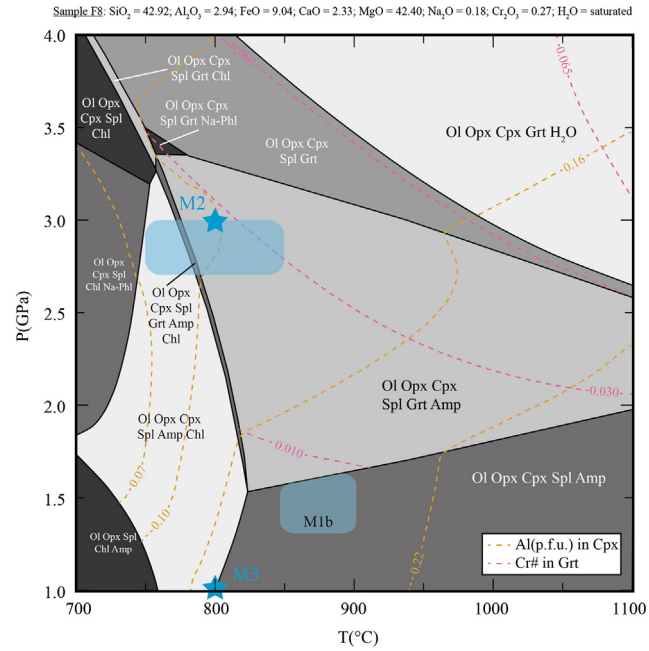

Fig. 11. PT section calculated using the Perple_X thermodynamic software (Connolly, 2005; version 6.6.8) with isopleths for Cr# (Cr/(Al + Cr)) in garnet and Al (p.f.u.) content in clinopyroxene. M2 mineral assemblage in the Cr-NCFMASH system. The M1b geothermometry is shown by the shaded area while the star symbols indicate PT conditions for the M2 and M3 mineral assemblage recorded in a cross-cutting eclogitic dyke (Janák et al., 2013).

Most likely, fluids hydrated the peridotite at the early Caledonian plate interface (which correspond here with M1b), before or during incorporation of the FGP in the subducting continental crust. This hypothesis is strengthened by the trails of Sr-bearing fluid inclusions (now mainly carbonates) lined up along optically visible defect boundaries within strongly deformed M1a–b mineral assemblages. Moreover, these fluid inclusions form minor phases within the M2 assemblage (Olfert, 2014).

7.1.3. M2

The M2 mineral assemblage overprints the lower pressure M1b kelyphite as well as the large outer globular M1b spinels surrounded by the M1b kelyphite. The M2 stage records intense deformation (D2), as reflected by the much smaller grain size of the M2 assemblage compared to the size of M1a minerals.

The M2 peak metamorphic conditions in peridotite are 2.9 ± 0.1 GPa–800 ± 50 °C. These results are strikingly similar to the M2 stage recorded within the eclogitic dyke cross-cutting the peridotite (3.0–3.5 GPa/750–850 °C; Janák et al., 2013).

7.1.4 . Post-M2

The D2 deformation phase that was associated with early-Caledonian (Jämtlandian; Brueckner and Van Roermund, 2004) subduction was strongly penetrative and affected the entire FGP body. The non-penetrative D3 deformation formed anastomosing shear zones within the stability field of the M3 mineral assemblage Ol + Opx + Cpx + Chl + Amph + Spl (i.e. at lower PT conditions than that for M2).

Mineral reactions were probably assisted by local hydration of portions of the rock volume. Furthermore, the much finer lamellar size of the M3 kelyphite (Fig. 2a–b–c) compared to that of the M1b kelyphite (Fig. 3a–b) indicates a lower temperature of formation. The M3 phase represents a decompression of the garnet peridotite which post-dated the early-Caledonian UHP event. The internal eclogitic dyke also records the isothermal decompression period post-dating the M2 UHP event.

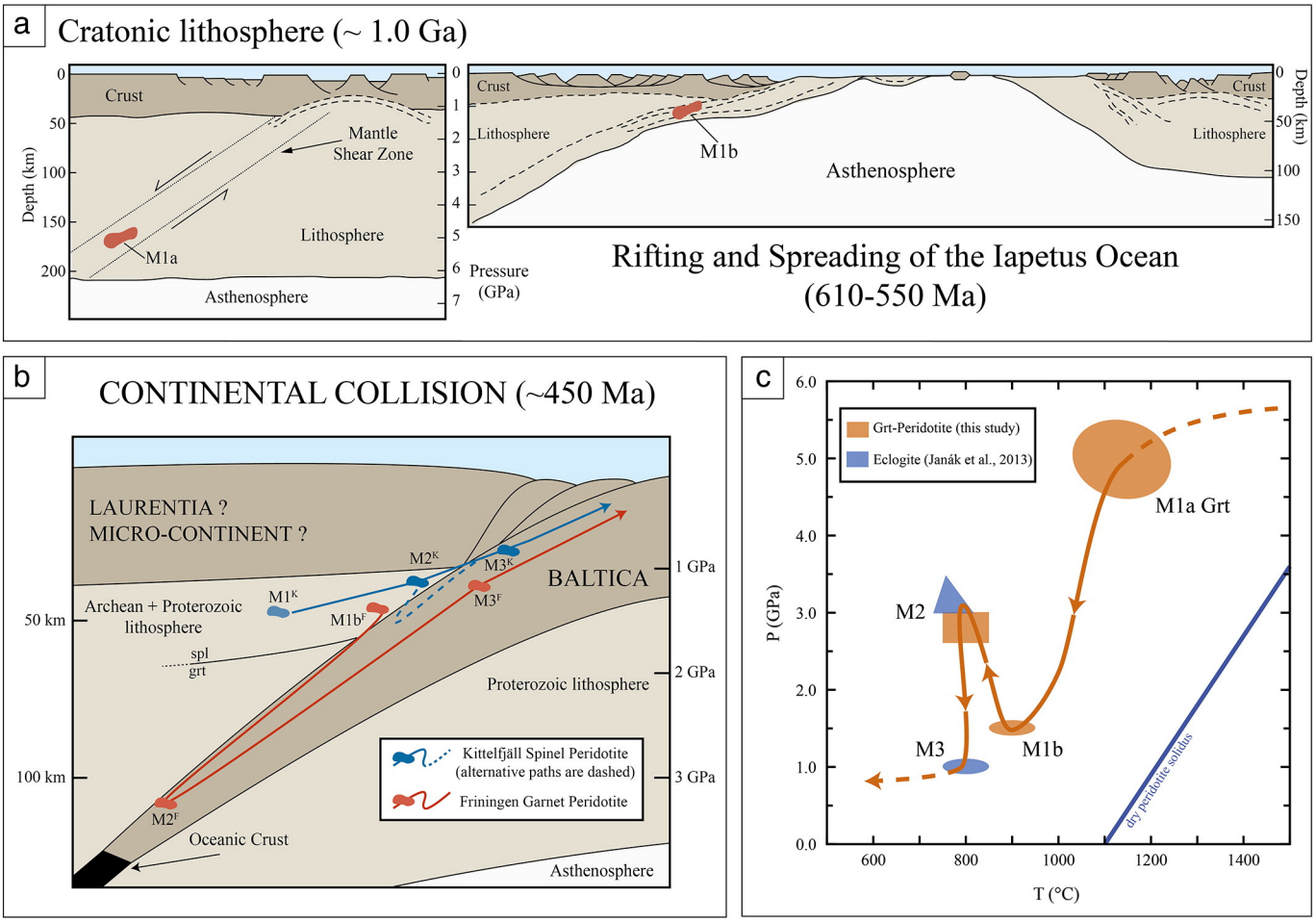

Fig. 12. a) Simplified cartoon illustrating the extensional phase related to Iapetus spreading interpreted to be responsible for the near-isothermal decompression of the FGP. b) Simplified cartoon illustrating geodynamic evolution of KSP and FGP in relation with the subducted SNC. FGP is crustally emplaced in the down-going slab during subduction and KSP during eduction of the SNC (discussion on alternative path of the KGP in Clos et al., 2014). c) Schematic PT path which portrays the potential evolution of the FGP.

Janák et al. (2013) calculated PT conditions of about 1.0–0.8GPa/750–850 °C. This M3 decompressional stage is also recorded in eclogites enclosed within the migmatitic gneisses of the Ertsekey lens (Joanny et al., 1991; Van Roermund, 1985).

7.2. Tectonic Implications

Brueckner and Van Roermund (2004) interpreted FGP as an orogenic garnet peridotite originating from a cold and thick lithospheric mantle wedge, positioned underneath either Laurentia or a micro-continent located between Baltica and Laurentia. The very deep (5.0 ± 1.0 GPa) and relatively cold (1100 ± 100 °C) formation conditions of the M1a garnet-bearing ultramafic assemblage supports this hypothesis. The M1a assemblage, including the primary assemblages (M1) of the eclogitic dyke, is probably the result of a Proterozoic recrystallization event (~1.2–1.1 Ga) related to partial refertilization of an Archean dunite body, positioned close to the base of a cold, thick and old lithosphere that was intruded by a dyke "swarm". Absolute timing of the M1b assemblage (decompression and cooling event) is uncertain, but is interpreted to be related to asymmetrical extension associated with Iapetus Ocean spreading (570–550 Ma; Fig. 12a). Alternatively, though less likely, the M1b stage might be related to an older (Proterozoic) decompression event.

The multiphase solid and fluid inclusions within M1a and M2 mineral assemblages provide the microstructural evidence that the FGP resided at the plate interface during early-Caledonian continental subduction to UHP metamorphic conditions (Janák et al., 2013).

Based on these observations, it appears that the FGP accompanied the surrounding Ertsekey lens of the SNC during "early-Caledonian" deep subduction. However, it remains uncertain how time was distributed among 1) early Caledonian subduction, 2) early Caledonian stalling, and 3) early Caledonian eduction. Regardless, the FGP resided at UHP depths long enough to allow the M2 UHP mineral assemblages to be formed.

The early-Caledonian near-isothermal decompression event M3 (Janák et al., 2013; 1.0–0.8 GPa/750–850 °C) most likely preceded a final cooling phase recorded in the surrounding gneisses. In effect, the country rock gneisses formed a soft and ductile matrix in which the FGP body acted mechanically as a relatively rigid body, escaping further retrogression under ambient PT conditions.

This newly documented PTt-d path of the FGP, illustrated in Fig. 12c, is typical for a mantle wedge garnet peridotite (MWgp; Van Roermund, 2009). It also resembles the PTt paths of the cold and old mantle wedge garnet peridotites of the Western Gneiss Complex, SW Norway, except of course for their subduction age (Brueckner et al., 2010; Zhang et al., 2011).

Several other orogenic peridotite bodies are found within the SNC of central Sweden (Zwart, 1974). A systematic study of the timing and crustal emplacement mechanisms of these orogenic peridotite bodies may provide a broader view on the tectonic evolution of the SNC during early-Caledonian times. Moreover most (if not all) orogenic peridotite bodies that are located within the upper and lower belts of the SNC are members of ophiolite complexes (Andersen et al., 2012; Williams and Zwart, 1977; Zwart, 1974). However to demonstrate that MW

garnet peridotites, as typified by the FGP, form a characteristic feature of the central/middle belt of the SNC in central Sweden it is necessary to refer to another orogenic peridotite body exposed in the central belt of the SNC in central Sweden, the Kittelfjäll Spinel Peridotite (KSP).

The KSP shows comparable microstructures and PT histories as the FGP. This orogenic spinel peridotite, located approximately 50 km north of FGP, belongs also to the Central/Middle Belt of the SNC (Clos et al., 2014). The country rock around the KSP consists of a migmatitic Ky + Kfs + Bt gneiss (Marsfjäll gneiss) and Grt–Cpx–Pl bearing amphibolite (Kittelfjäll amphibolite). Similarly to the FGP, the KSP shows three contrasting olivine microstructures; large (up to 20 cm) M1 olivine porphyroclasts surrounding M2 olivine foam microstructures and a third olivine (1–50 μm) within M3 shear zones. Both the KSP and the FGP are interpreted to be mantle wedge peridotites with subcontinental affinity and a roughly similar early-Caledonian PTt-d path (Clos et al., 2014; Fig. 12b). However, the PTt-d path of both mantle wedge peridotite bodies differs in their early-Caledonian evolution and crustal incorporation history, as the KSP was probably emplaced during eduction from the Laurentian (or micro-continental) mantle wedge (hanging wall). In contrast, the FGP was first incorporated in subducted continental crust and subsequently experienced prograde metamorphism culminating in early Caledonian (Jämtlandian?) UHP metamorphism and then educted.

The combined PTt-d paths of the FGP and KSP provide important insights into the role of the SNC during early-Caledonian and Scandian collisions between Baltica and Laurentia. Based on the many similarities with the WGR, we consider the (U)HP rocks of the central belt of the SNC to represent parts of the most external part of Baltica (Gee et al., 2013). This terrane subducted, detached, educted and back-thrusted over the sedimentary cover of the middle allochthon before the WGR reached the Scandian UHPM peak. However, further investigations on the timing and crustal emplacement mechanisms of other ultramafic bodies within the SNC of central Sweden should be carried out to solve the fundamental question of how two different types of orogenic peridotites can be systematically mixed on a regional scale across the SNC. We believe that such investigations will produce new and alternative ways to find answers regarding formation of the SNC in central Sweden in Caledonian time.

8. Conclusions

1) Pre-Caledonian UHP-HT metamorphic conditions of 1100 ± 100 °C and 5.0 ± 0.5 GPa are established for the early M1a garnet-bearing mineral assemblage. These physical conditions were followed by decompression related to inferred late Proterozoic exhumation recorded at 850–900 °C and 1.5 GPa (M1b).
2) At the onset of early Caledonian subduction and collision, the FGP resided at the plate interface between a mantle wedge and a subducting continental plate. During this early-Caledonian subduction event, crustal incorporation of FGP took place together with intense deformation and metasomatism by means of COH-rich subduction zone fluids.
3) Evidence for early Caledonian UHP conditions in the FGP is provided by the M2 assemblage of Ol + Opx + Cpx + Grt + Spl + Amp, which overprints the older M1a–b assemblage, and equilibrated at around 810 °C and 3.1 GPa. These conditions are closely comparable to those established for M2 recrystallization in an associated eclogitic dyke at 800 °C and 3.0 GPa (Gee et al., 2013; Janák et al., 2013).
4) Static re-equilibration of M2 Grt + Ol to M3 Opx + Spl + Amp kelyphite (Fig. 2c) is indicative of isothermal decompression down to 750–800 °C and 1.0–0.6 GPa (M3; Janák et al., 2013). This decompression event occurred in the absence of any optically recognisable penetrative deformation.
5) Based on the above points, and in agreement with the previously published age determinations (Brueckner et al., 2004), and previous geothermobarometry on associated metabasic rocks (Janák et al., 2013), we propose for the FGP a new, well-constrained PTt-d path (Fig. 12a–b–c) that is characteristic for a mantle wedge garnet peridotite.

Acknowledgement

The results presented in this paper form an upgraded version of a one-year MSc research project performed at the Structural Geology Group, Earth Science Department, Utrecht University, The Netherlands. A copy of the MSc thesis by M. Gilio can be downloaded from the Igitur-Archive, MSc theses, University Library, Utrecht University, The Netherlands. The authors gratefully thank Dr. Olivier Plümper for his help with the EBSD work on the fine-grained olivine M3 foam-like microstructure of sample F10. HvR would like to express his gratitude to Bill Griffin, Hannes Brueckner and the late Tony Carswell for "brainwashing and motivation", each in their own particular way as well as at different times in his life. Without their continuous inspiration, this manuscript would have never seen the sunlight. Moreover, we thank the two anonymous reviewers and Gordon Medaris for their comments and advice, which highly improved the quality of this work.

Appendix A. Supplementary data

Supplementary data to this article can be found online at http://dx.doi.org/10.1016/j.lithos.2015.05.003.

References

Andersen, T.B., Corfu, F., Labrousse, L., Osmundsen, P.T., 2012. Evidence for hyperextension along the pre-Caledonian margin of Baltica. Journal of the Geological Society 169 (5), 601–612.
Andréasson, P.G., 1994. The Baltoscandian Margin in Neoproterozoic–early Palaeozoic times. Some constraints on terrane derivation and accretion in the Arctic Scandinavian Caledonides. Tectonophysics 231, 1–32.
Ballhaus, C., Berry, R.F., Green, D.H., 1991. High pressure experimental calibration of the olivine–orthopyroxene–spinel oxygen geobarometer: implications for the oxidation state of the upper mantle. Contributions to Mineralogy and Petrology 107, 27–40.
Bebout, G.E., 2007. Metamorphic chemical geodynamics of subduction zones. Earth and Planetary Science Letters 260 (3-4), 373–393.
Benisek, A., Dachs, E., Kroll, H., 2010. Excess heat capacity and entropy of mixing in ternary series of high-structural-state feldspars. European Journal of Mineralogy 22 (3), 403–410.
Berman, R.G., Aranovich, L.Y., Pattison, D.R.M., 1995. Reassessment of the garnet–clinopyroxene Fe–Mg exchange thermometer: II. Thermodynamic analysis. Contributions to Mineralogy and Petrology 119, 30–42.
Bertrand, P., Merrier, J.C.C., 1985. The mutual solubility of coexisting ortho- and clinopyroxene: toward an absolute geothermometer for the natural system? Earth and Planetary Science Letters 76, 109–122.
Beyer, E.E., Griffin, W.L., O'Reilly, S.Y., 2006. Transformation of Archean lithospheric mantle by refertilization: evidence from exposed peridotites in the Western Gneiss Region, Norway. Journal of Petrology 47, 1611–1636.
Brenker, F.E., Brey, G.P., 1997. Reconstruction of the exhumation path of Alpe Arami garnet peridotite body from depths exceeding 160 km. Journal of Metamorphic Geology 15, 581–592.
Brey, G.P., Köhler, T., 1990. Geothermobarometry in four-phase lherzolites II. New thermobarometers, and practical assessment of existing thermobarometers. Journal of Petrology 31, 1353–1378.
Brey, G.P., Bulatov, V.K., Girnis, A.V., 2008. Geobarometry for peridotites: experiments in simple and natural systems from 6–10 GPa. Journal of Petrology 49, 3–24.
Brueckner, H.K., 1977. A crustal origin for eclogites and mantle origin for garnet peridotites: strontium isotopic evidence from clinopyroxenes. Contributions to Mineralogy and Petrology 60, 1–15.
Brueckner, H.K., 1998. Sinking intrusion model for the emplacement of garnet-bearing peridotites into continent collision orogens. Geology 26, 631–634.
Brueckner, H.K., Van Roermund, H.L.M., 2004. Dunk tectonics: a multiple subduction/eduction model for the evolution of the Scandinavian Caledonides. Tectonics 23, 1–20.
Brueckner, H.K., Van Roermund, H.L.M., 2007. Concurrent HP metamorphism on both margins of Iapetus: Ordovician ages for eclogites and garnet pyroxenites from the Seve Nappe Complex, Swedish Caledonides. Journal of the Geological Society, London 164, 117–128.
Brueckner, H.K., Carswell, D.A., Griffin, W.L., 2002. Palaeozoic diamonds within a Precambrian peridotite lens in UHP gneisses of the Norwegian Caledonides. Earth and Planetary Science Letters 203, 805–816.
Brueckner, H.K., Van Roermund, H.L.M., Pearson, N.J., 2004. An Archean (?) to Paleozoic evolution for a garnet peridotite lens with sub-Baltic shield affinity within the Seve

Nappe Complex of Jämtland, Sweden, Central Scandinavian Caledonides. Journal of Petrology 45, 415–437.
Brueckner, H.K., Carswell, D.A., Griffin, W.L., Medaris, L.G., Van Roermund, H.L.M., Cuthbert, S.J., 2010. The mantle and crustal evolution of two garnet peridotite suites from the Western Gneiss Region, Norwegian Caledonides: an isotopic investigation. Lithos 117, 1–19.
Bucher-Nurminen, K., 1991. Mantle fragments in the Scandinavian Caledonides. Tectonophysics 190 (2), 173–192.
Carlson, W.D., 2006. Rates of Fe, Mg, Mn, and Ca diffusion in garnet. American Mineralogist 91 (1), 1–11.
Carswell, D.A., Harvey, M.A., Al-Samman, A., 1983. The petrogenesis of contrasting Fe–Ti and Mg–Cr garnet peridotite types in the high grade gneiss complex of Western Norway. Bulletin de Mineralogie 106, 727–750.
Chatterjee, N.D., Leistner, H., Terhart, L., Abraham, K., Klaska, R., 1982. Thermodynamic mixing properties of corundum eskolaite, alpha-(Al, Cr^{+3})2O3, crystalline solutions at high-temperatures and pressures. American Mineralogist 67, 725–735.
Clos, F., Gilio, M., Van Roermund, H.L.M., 2014. Fragments of deeper parts of the hanging wall mantle preserved as orogenic peridotites in the central belt of the Seve Nappe Complex, Sweden. Lithos 192–195, 8–20.
Coleman, R.G., 1971. Plate tectonic emplacement of upper mantle peridotites along continental edges. Journal of Geophysical Research 76 (5), 1212–1222.
Connolly, J.A.D., 2005. Computation of phase-equilibria by linear programming: a tool for geodynamic modelling and its application to subduction zone decarbonation. Earth and Planetary Science Letters 236, 524–541.
Dale, J., Holland, T., Powell, R., 2000. Hornblende–garnet–plagioclase thermobarometry: a natural assemblage calibration of the thermodynamics of hornblende. Contributions to Mineralogy and Petrology 140 (3), 353–362.
Den Tex, E., 1969. Origin of ultramafic rocks, their tectonic setting and history. Tectonophysics 7, 457–488.
Du Rietz, T., 1935. Peridotites, serpentinites and soapstones of northern Sweden. Geologiska Föreningens i Stockholm Förhandlingar 57/2, 133–260.
Ellis, D.J., Green, D.H., 1979. An experimental study of the effect of Ca upon garnet–clinopyroxene Fe–Mg exchange equilibria. Contributions to Mineralogy and Petrology 71, 13–22.
Eskola, P., 1921. On the eclogites of Norway. Skr. Vidensk. Selsk. Christiania, Mat.-Nat. Kl. I 8 pp. 1–118.
Gee, D.G., Fossen, H., Henriksen, N., Higgins, A.K., 2008. From the early Paleozoic platforms of Baltica and Laurentia to the Caledonide Orogen of Scandinavia and Greenland. Episodes 31 (1), 44.
Gee, D.G., Marian, J., Majka, J., Robinson, P., Van Roermund, H.L.M., 2013. Subduction along and within the Baltoscandian margin during the closing of the Iapetus Ocean and Baltica–Laurentia collision. Lithosphere 5, 169–178.
Harley, S.L., 1984. An experimental study of the partitioning of Fe and Mg between garnet and orthopyroxene. Contributions to Mineralogy and Petrology 86, 353–373.
Holland, T.J.B., Powell, R., 1996. Thermodynamics of order–disorder in minerals. 2. Symmetric formalism applied to solid solutions. American Mineralogist 81, 1425–1437.
Holland, T.J.B., Powell, R., 1998. An internally consistent thermodynamic data set for phases of petrological interest. Journal of Metamorphic Geology 16, 309–344.
Jamtveit, B., 1987. Metamorphic evolution of the Eiksunddal eclogite complex. Western Norway, and some tectonic implications. Contributions to Mineralogy and Petrology 95 (1), 82–99.
Janák, M., Van Roermund, H.L.M., Majka, J.C., Gee, D.G., 2013. UHP metamorphism recorded by kyanite-bearing eclogite in the Seve Nappe Complex of northern Jämtland, Swedish Caledonides. Gondwana Research 23 (3), 865–879.
Joanny, V., Van Roermund, H.L.M., Lardeaux, L.M., 1991. The clinopyroxene/plagioclase symplectite in retrograde eclogites: a potential geothermobarometer. Geologische Rundschau 80, 303–320.
Klemme, S., 2010. Experimental constraints on the evolution of iron and phosphorus-rich melts: experiments in the system CaO–MgO–Fe2O3–P2O5–SiO2–H2O–CO2. Journal of Mineralogical and Petrological Sciences 105 (1), 1–8.
Krogh, E.J., 1988. The garnet–clinopyroxene Fe–Mg–geothermometer—a reinterpretation of existing experimental data. Contributions to Mineralogy and Petrology 99, 44–48.
Krogh, E.J., Kullerud, K., Ellingsen, E., 2006. Prograde garnet-bearing ultramafic rocks from the Tromsø Nappe, northern Scandinavian Caledonides. Lithos 92, 336–356.
Krogh-Ravna, E.J., 2000. The garnet–clinopyroxene Fe^{2+}–Mg geothermometer: an updated calibration. Journal of Metamorphic Geology 18, 211–219.
Krogh-Ravna, E.J., Paquin, J., 2003. Thermobarometric methodologies applicable to eclogites and garnet peridotites. In: Carswell, D.A., Compagnoni, R. (Eds.), Ultrahigh Pressure Metamorphism. EMU Notes in Mineralogy 5. Eötvös University Press, Budapest, Hungary, pp. 229–259.
Kühn, A., Glodny, J., Iden, K., Austrheim, H., 2000. Retention of Precambrian Rb/Sr phlogopite ages through Caledonian eclogite facies metamorphism, Bergen Arc Complex, W-Norway. Lithos 51 (4), 305–330.
Leake, B.E., Woolley, A.R., Arps, C.E.S., Birch, W.D., Gilbert, M.C., Grice, J.D., Hawthorne, F.C., Kato, A., Kisch, H.J., Krivovichev, V.G., Linthout, K., Laird, J., Mandarino, J.A., Maresch, W.V., Nickel, E.H., Rock, N.M.S., Schumacher, J.C., Smith, D.C., Stephenson, N.C.N., Ungaretti, L., Whittaker, E.J.W., Youzhi, G., 1997. Nomenclature of amphiboles: report of the subcommittee on amphiboles of the International Mineralogical Association, commission on new minerals and mineral names. Canadian Mineralogist 35, 219–246.
MacGregor, I.D., 1974. The system MgO–Al2O3–SiO2: solubility of Al2O3 in enstatite for spinel and garnet peridotite compositions. American Mineralogist 59, 110–119.
Majka, J., Janák, M., Andersson, B., Klonowska, I., Gee, D.G., Rosén, Å., Kośmińska, K., 2013. Pressure temperature estimates on the Tjeliken eclogite: new insights into (ultra)-high pressure evolution of the Seve Nappe Complex in the Scandinavian Caledonides. Geological Society, Special Publication 390, 369–384.
Mattioli, G.S., Bishop, F.C., 1984. Experimental-determination of the chromium–aluminum mixing parameter in garnet. Geochimica et Cosmochimica Acta 48, 1367–1371.
Medaris, L.G., 1984. A geothermobarometric investigation of garnet peridotites in the Western Gneiss Region of Norway. Contributions to Mineralogy and Petrology 87 (1), 72–86.
Nakamura, D., Hirajima, T., 2005. Experimental evaluation of garnet–clinopyroxene thermometry as applied to eclogites. Contributions to Mineralogy and Petrology 150, 581–588.
Nickel, K.G., Green, D.H., 1985. Empirical geothermobarometry for garnet peridotites and implications for the nature of the lithosphere, kimberlites and diamonds. Earth and Planetary Science Letters 73, 158–170.
Nicolas, A., Poirier, J.P., 1976. Crystalline Plasticity and Solid State Flow in Metamorphic Rocks. Wiley, New York.
Nimis, P., Taylor, W.R., 2000. Single clinopyroxene thermobarometry for garnet peridotites. Part I. Calibration and testing of a Cr-in-Cpx barometer and an enstatite-in-Cpx thermometer. Contributions to Mineralogy and Petrology 139, 541–554.
O'Neill, H.S.C., Wood, B.J., 1979. An experimental study of Fe–Mg partitioning between garnet and olivine and its calibration as a geothermometer. Contributions to Mineralogy and Petrology 70, 59–70.
Obata, M., Morten, L., 1987. Transformation of spinel lherzolite to garnet lherzolite in ultramaphic lenses of the austridic crystalline complex, Northern Italy. Journal of Petrology 28, 599–623.
Olfert, N., 2014. An Investigation of the Origin of Multiphase Solid Inclusions Within Minerals of the Friningen Garnet Peridotite, N.Jamtland, Central Sweden. (MSc thesis), Utrecht University (on request by Igitur-Archive, MSc theses, University Library, Utrecht University, the Netherlands).
O'Neill, H.S.C., 1980. An experimental study of the iron–magnesium partitioning between garnet and olivine and its calibration as a geothermometer: corrections. Contributions to Mineralogy and Petrology 72, 337.
O'Neill, H.S.C., Wall, V.J., 1987. The olivine–orthopyroxene–spinel oxygen geobarometer, the nickel precipitation curve, and the oxygen fugacity of the Earth's upper mantle. Journal of Petrology 28, 1169–1191.
Powell, R., 1985. Regression diagnostics and robust regression in geothermometer/geobarometer calibration: the garnet–clinopyroxenc geothermometer revisited. Journal of Metamorphic Geology 3, 231–243.
Qvale, H., Stigh, J., 1985. Ultramafic rocks in the Scandinavian Caledonides. In: Gee, D.G., Sturt, B.A. (Eds.), The Caledonide Orogen: Scandinavia and Related Areas. Wiley, New York, pp. 693–715.
Ryan, C.G., Griffin, W.L., Pearson, N.J., 1996. Garnet geotherms: pressure–temperature data from Cr-pyrope garnet xenocrysts in volcanic rocks. Journal of Geophysical Research 101, 5611–5625.
Scambelluri, M., Hermann, J., Morten, L., Rampone, E., 2006. Melt- versus fluid-induced metasomatism in spinel to garnet wedge peridotites (Ulten Zone, Eastern Italian Alps): clues from trace element and Li abundances. Contributions to Mineralogy and Petrology 151, 372–394.
Scambelluri, M., Van Roermund, H.L., Pettke, T., 2010. Mantle wedge peridotites: fossil reservoirs of deep subduction zone processes: inferences from high and ultrahigh-pressure rocks from Bardane (Western Norway) and Ulten (Italian Alps). Lithos 120 (1), 186–201.
Scambelluri, M., Pettke, T., Rampone, E., Godard, M., Reusser, E., 2014. Petrology and trace element budgets of high-pressure peridotites indicate subduction dehydration of serpentinized mantle (Cima di Gagnone, Central Alps, Switzerland). Journal of Petrology 55 (3), 459–498.
Spengler, D., 2006. Origin and evolution of deep upper mantle rocks from western Norway. Geologica Ultrajectina 266. V, Utrecht University, The Netherlands.
Spengler, D., Van Roermund, H.L.M., Drury, M.R., Ottolini, L., Mason, P.R.D., Davies, G.R., 2006. Deep origin and hot melting of an Archean orogenic peridotite massif in Norway. Nature 440, 913–917.
Spengler, D., Brueckner, H.K., Van Roermund, H.L.M., Drury, M.R., Mason, P.R.D., 2009. Long-lived, cold burial of Baltica towards 200 km depth. Earth and Planetary Science Letters 281, 27–35.
Strömberg, A.G.B., Karis, L., Zachrisson, E., Sjöstrand, T., Skoglund, R., 1984. Bedrock Geological Map of Jämtland County (Caledonides), scale 1:200 000. Sveriges Geologiska Undersökning Ca 53.
Taylor, W.R., 1998. An experimental test of some geothermometer and geobarometer formulations for upper mantle peridotites with application to the thermobarometry of fertile lherzolite and garnet websterite. Neues Lehrbuch fur Mineralogie, Abhandlungen 172, 381–408.
Trommsdorff, V., Evans, B.W., 1974. Alpine metamorphism of peridotitic rocks. Schweizerische Mineralogische und Petrographische Mitteilungen 54, 333–352.
Trouw, R.A.J., 1973. Structural geology of the Marsfjällen area Caledonides of Västerbotten Sweden, Sveriges Geologiska Undersökning, Ser. C. Nr. 689. Årsbok 67 (7).
Van Roermund, H.L.M., 1985. Eclogites of the Seve nappe, central Scandinavia Caledonides. In: Gee, D.G., Sturt, B.A. (Eds.), The Caledonide Orogen — Scandinavia and Related Areas, pp. 873–886.
Van Roermund, H.L.M., 1989. High-pressure ultramafic rocks from the allochthonous nappes of the Swedish Caledonides. In: Grayer, R.A. (Ed.), The Caledonide Geology of Scandinavia. Graham and Trotman, London, pp. 205–219.
Van Roermund, H.L.M., 2009. Mantle-wedge garnet peridotites from the northernmost ultra-high pressure domain of the Western Gneiss Region, SW Norway. European Journal of Mineralogy 21, 1085–1096.
Van Roermund, H.L.M., Bakker, E., 1984. Structure and metamorphism of the Tängen-Inviken area, Seve Nappes, central Scandinavian Caledonides. Geologiska Föreningens i Stockholm Förhandlingar 105, 301–319.

Van Roermund, H.L.M., Drury, M.R., 1998. Ultra-high pressure (P > 6 GPa) garnet peridotites in Western Norway: exhumation of mantle rocks from >185 km depth. Terra Nova 10, 295–301.
Verbaas, J., Van Roermund, H.L.M., 2012. The Tectonometamorphic Evolution of the Friningen Peridotite Lens: Sub-Continental Lithospheric Mantle Exposed at the Surface in the Seve Nappe Complex of the Scandinavian Caledonides. LAP LAMBERT Academic Publishing (132 pp.).
Whitney, D., Evans, P., 2010. Abbreviations for names of rock-forming minerals. American Mineralogist 95, 185–187.
Williams, P.F., Zwart, H.J., 1977. A model for the development of the Seve-Köli Caledonian Nappe Complex. In: Saxena, S.K., Bhattacharji, S. (Eds.), Energetics of Geological Processes. Springer Verlag, New York, pp. 169–187.
Witt-Eickschen, G., Seck, H.A., 1991. Solubility of Ca and Al in Orthopyroxene from spinel peridotite — an improved version of an empirical geothermometer. Contributions to Mineralogy and Petrology 106, 431–439.
Wu, C.M., Zhao, G.C., 2007. A recalibration of the garnet-olivine geothermometer and a new geobarometer for garnet peridotites and garnet-olivine-plagioclase-bearing granulites. Journal of Metamorphic Geology 25, 497–505.
Zachrisson, E., 1969. Caledonian Geology of Northern Jämtland-Southern Västerbotten: Köli Stratigraphy and Main Tectonic Outlines. Svensk reproduktions AB.
Zachrisson, E., Stephens, M.B., 1984. Mega-structures within the Seve Nappes, southern Norrbotten Caledonides, Sweden. Meddelanden från Stockholms Universitets Geologiska Institution 255 p. 241.
Zhang, C., Van Roermund, H.L.M., Zhang, L.F., 2011. Orogenic garnet peridotites: tools to reconstruct paleo-geodynamic settings of fossil continental collision zones. Ultrahigh Pressure Metamorphism, 25 Years After the Discovery of Coesite and Diamond, London, pp. 501–539.
Zheng, Y.F., 2012. Metamorphic chemical geodynamics in continental subduction zones. Chemical Geology 328, 5–48.
Ziberna, L., Klemme, S., Nimis, P., 2013. Garnet and spinel in fertile and depleted mantle: insights from thermodynamic modelling. Contributions to Mineralogy and Petrology 166 (2), 411–421.
Zwart, H.J., 1974. Structure and metamorphism in the Seve-Köli Nappe Complex (Scandinavian Caledonides) and its implications concerning the formation of metamorphic nappes. In: Bellière, J., Duchesne, J.C. (Eds.), Géologie des Domains Cristallins. Centenaire de la Société Géologique de Belgique, Liège, pp. 129–144.